THE JOURNAL OF PHYSICAL CHEMISTRY B

Article

Cite This: J. Phys. Chem. B 2018, 122, 4051−4066

pubs.acs.org/JPCB

Radical Ions of 3-Styryl-quinoxalin-2-one Derivatives Studied by Pulse Radiolysis in Organic Solvents

Konrad Skotnicki,[†] Julio R. De la Fuente,*[,‡] Álvaro Cañete,[§] Eduardo Berrios,[‡] and Krzysztof Bobrowski*[,†,∥]

[†]Institute of Nuclear Chemistry and Technology, 03-195 Warsaw, Poland

[‡]Departamento de Química Orgánica y Fisicoquímica, Facultad de Ciencias Químicas y Farmacéuticas, Universidad de Chile, Casilla 223, Santiago 1 8380492, Chile

[§]Departamento de Química Orgánica, Facultad de Química, Pontificia Universidad Católica de Chile, Casilla 306, Correo 22, Santiago 7820436, Chile

[∥]Notre Dame Radiation Laboratory, University of Notre Dame, Notre Dame, Indiana 46556, United States

Supporting Information

ABSTRACT: The absorption-spectral and kinetic behaviors of radical ions and neutral hydrogenated radicals of seven 3-styryl-quinoxalin-2(1*H*)-one (3-SQ) derivatives, one without substituents in the styryl moiety, four others with electron-donating (R = $-CH_3$, $-OCH_3$, and $-N(CH_3)_2$) or electron-withdrawing (R = $-OCF_3$) substituents in the para position in their benzene ring, and remaining two with double methoxy substituents ($-OCH_3$), however, at different positions (meta/para and ortho/meta) have been studied by UV−vis spectrophotometric pulse radiolysis in neat acetonitrile saturated with argon (Ar) and oxygen (O_2) and in 2-propanol saturated with Ar, at room temperature. In acetonitrile solutions, the radical anions (4R-SQ$^{\bullet-}$) are characterized by two absorption maxima located at λ_{max} = 470−490 nm and λ_{max} = 510−540 nm, with the respective molar absorption coefficients $\varepsilon_{470-490}$ = 8500−13 100 M^{-1} cm^{-1} and $\varepsilon_{510-540}$ = 6100−10 300 M^{-1} cm^{-1}, depending on the substituent (R). All 4R-SQ$^{\bullet-}$ decay in acetonitrile via first-order kinetics, with the rate constants in the range (1.2−1.5) × 10^6 s^{-1}. In 2-propanol solutions, they decay predominantly through protonation by the solvent, forming neutral hydrogenated radicals (4R-SQH$^{\bullet}$), which are characterized by weak absorption bands with λ_{max} = 480−490 nm. Being oxygen-insensitive, the radical cations (4R-SQ$^{\bullet+}$) are characterized by a strong absorption with λ_{max} = 450−630 nm, depending on the substituent (R). They are formed in a charge-transfer reaction between a radical cation derived from acetonitrile (ACN$^{\bullet+}$) and substituted 3-styryl-quinoxalin-2-one derivatives (4R-SQ) with a pseudo-first-order rate constant k = (2.7−4.7) × 10^5 s^{-1} measured in solutions containing 0.1 mM 4R-3-SQ. The Hammett equation plot gave a very small negative slope (ρ = −0.08), indicating a very weak influence of the substituents in the benzene ring on the rate of charge-transfer reaction. The decay of 4R-SQ$^{\bullet+}$ in Ar-saturated acetonitrile solutions occurs with a pseudo-first-order rate constant k = (1.6−6.2) × 10^4 s^{-1} and, in principle, is not affected by the presence of O_2, suggesting charge−spin delocalization over the whole 3-SQ molecule. Most of the radiolytically generated transient spectra are reasonably well-reproduced by semiempirical PM3-ZINDO/S (for 4R-SQ$^{\bullet-}$) and density functional theory quantum mechanics calculations employing M06-2x hybrid functional together with the def2-TZVP basis set (for 4R-SQ$^{\bullet+}$).

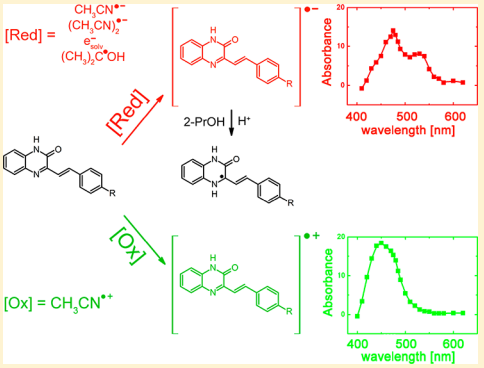

INTRODUCTION

Quinoxaline derivatives have received a wide attention in the past and in the current decade of the 21st century because of their numerous and broad applications.[1] They are found to be important in industry because of their ability to inhibit metal corrosion.[2] The quinoxaline structure acts as a precursor to assemble a large number of new compounds for luminescent materials because of the π-deficient character of the quinoxaline ring, leading to significant modifications of the photophysical properties of π-conjugated materials. The electron deficiency of the quinoxaline ring favors internal charge transfer facilitating dipole formation. These molecules exhibit important solvatochromism and good nonlinear optical properties. Moreover, the quinoxaline rings, because of the presence of nitrogen atoms with lone electron pairs, can act as effective and stable complexing agents, making them good cation sensors or making them halochromic on protonation.[3] Some quinoxaline derivatives were also used as electron-transporting or hole-blocking materials in organic light-emitting devices[4−7] and in organic thin-film transistors.[8]

Received: January 29, 2018
Revised: March 9, 2018
Published: March 13, 2018

DOI: 10.1021/acs.jpcb.8b01004
J. Phys. Chem. B 2018, 122, 4051−4066

However, a recent update of the literature has shown that quinoxaline derivatives, those of quinoxaline-2-one in particular, attracted attention, primarily because of their tremendously wide spectrum of biological activities.[1,9,10] They were found as anti-HIV agents;[11,12] aldose reductase,[13,14] cyclin-dependent kinase,[15] monoamine oxidase A,[16] SR protein-specific kinase-1,[17] and glycogen phosphorylase inhibitors;[18] angiotensin II receptor and multiple-drug-resistance antagonists;[19,20] 5-HT3 receptor agonists;[21] and GABA/benzodiazepine receptor ligands.[11,22−25] Nearly, all of the derivatives that have biological activities contain a substituent in position 3 of the pyrazine ring of quinoxalin-2-one.

The biological activities of this class of compounds are closely related to their pharmaceutical applications. They are effective as antibacterial, antiparasitic, antifungal, analgesic, antimalarial, antitumor, antiamoebic, antiepileptic, anticonvulsant, antitubercular, antiproliferative, and anti-inflammatory agents.[1,9,10]

Recently, great attention has been paid to 3-styryl-quinoxaline derivatives containing additional substituents in various positions of the pyrazine ring. They were found to be a class of compounds that can be potentially very effective in therapeutic medicine. Selected examples include two 3-styryl-quinoxaline derivatives containing *p*-methoxystyryl and *p*-fluorostyryl side chains with tetrazolo substituents at N1 and C2, which exhibit promising activity as potent anticonvulsants,[26] and 3-styryl-quinoxaline and 3-(2-hydroxystyryl)-quinoxaline with a thioether substituent at C2, which showed some improved antitumor activity, which qualified them for further study in antitumor drug design.[27]

Very recently, attention has been paid to amphiphilic 3-styryl-quinoxaline-2-one alkoxy derivatives, with different alkyl chain lengths at the position 4 of the alkoxy moiety, which are widely used dye molecules owing to their acidichroism and photochemical sensitivities.[28−30] They were found to undergo predominantly reversible trans−cis isomerization in solution,[30] whereas in Langmuir−Blodgett films [2,2], photodimerization was found as the preferred reaction pathway.[28] Interestingly, it was observed that the photodimerization kinetics is correlated with surface morphologies and its rate constant decreased significantly with the acidity.[29]

The 3-styryl-quinoxalin-2-one containing a *p*-dimethylaminestyryl side chain has been recently tested as a new fluorescent probe for amyloid-*β*-fibrils, which can be considered as a promising staining tool for the detection and study of peptide/protein aggregation.[31] This approach can be very useful for the diagnosis of neurodegenerative diseases including prion, Parkinson's, Huntington's, and Alzheimer's diseases, in which peptide/protein aggregation has been postulated.

Interestingly, four 3-styryl-quinoxalin-2-one derivatives (found to be very effective in therapeutic medicine as aldose reductase inhibitors) expressed additionally very high radical-scavenging activity.[14] These include two 3-styryl-quinoxalin-2-one derivatives containing *p*-hydroxystyryl side chains, a 3-styryl-quinoxalin-2-one derivative with a *p*-methoxystyryl side chain, and a 3-styryl-quinoxalin-2-one derivative with a 3-methoxy,4-hydroxystyryl side chain. This was shown especially for the latter derivative by the very effective DPPH radical scavenging (comparable with trolox) and by suppressing lipid peroxidation. In particular, the *p*-hydroxystyryl side chain attached to the C3 atom was identified as the key motif in quinoxalin-2-one compounds for their antioxidant activity. Thus, these compounds can potentially increase intracellular antioxidant defense during oxidative stress when there is an accumulation of excess reactive oxygen species resulting in the oxidative degradation of vital biomolecules. Moreover, a structure−activity relationship analysis combined with docking studies showed that one of these 3-styryl-quinoxalin-2-one derivatives containing a *p*-hydroxystyryl side chain was especially tightly bound in the active site of aldose reductase.[14] Interestingly, this side chain formed a stable stacking interaction with the indole ring of the Trp111 and was well-placed in the pocket formed by the side chains of Trp111, Leu300, Phe122, Cys303, Thr113, Phe115, and Trp79.[32] In addition, the quinoxalin-2-one moiety matched very well the hydrophobic pocket that contains, on its surface, the side chains of Leu300, Trp219, Phe122, Trp20, and Trp79. The fact that this compound is bound in such a specific position in the protein may have serious consequences in its interaction with either amino acid residues or radicals derived from it. Two amino acid residues tryptophan (Trp) and cysteine (Cys) are particularly vulnerable to oxidation. Therefore, either the radical cations derived from 3-styryl-quinoxalin-2-ones can oxidize them to tryptophyl ($TrpN^{\bullet}$) and thiyl ($CysS^{\bullet}$) radicals or the radicals derived from the surrounding amino acid residues can act as oxidants or reductants of quinoxalin-2-ones intercalated into the protein matrix.

The examples given above, showing the broad application of 3-styryl-quinoxalin-2-one derivatives as electron-transporting or hole-blocking materials as well their high antioxidant activity and specific docking in proteins, strongly indicate the need to characterize the spectral and kinetic properties of radicals and radical ions derived from them. In addition, knowledge regarding the spectral and kinetic behavior of radical anions and hydrogenated radicals of 3-styryl-quinoxalin-2-one derivatives will become necessary in interpreting some of the transient phenomena observed by us during photoreduction of these compounds by selected amino acids.

In the last few years, identification of radical and radical-ion species derived from some selected quinoxaline-2-ones was performed using pulse radiolysis in aqueous solutions.[33,34] In turn, pulse radiolysis generation of radical cations of stilbene derivatives (which can be also treated as styryl-substituted benzenes) was successfully accomplished in 1,2-dichloroethane and *n*-butyl chloride.[35,36]

In principle, pulse radiolysis offers a convenient method for generating radical ions and excited states or preferentially one of them, depending on the solvent used and the saturating gas. For instance, acetonitrile was used for the pulse radiolytic generation of radical cations as well as radical anions derived from the appropriately chosen solutes.[37−43] Pulse irradiation of neat acetonitrile leads to the formation of acetonitrile positive ions and classical solvated electrons (dipole-bound excess electrons) in dynamic equilibrium with dimeric radical anions $(CH_3CN)_2^{\bullet-}$ (valence-bound excess electrons).[44−47] Therefore, in this solvent saturated with Ar, both radical ions of the solute can be formed, whereas in O_2-saturated acetonitrile, only radical cations are formed. On the other hand, 2-propanol was used for selective pulse radiolytic generation of radical anions derived from the solutes.[37,48,49] In this polar protic solvent, radical anions are formed through the attachment of the solvated electrons (e_{solv}^-) to the solute molecule. Solute radical cations, however, are not formed because the alcohol-derived positive radical cations disappear very fast, producing strongly reductive ketyl radicals ($(CH_3)_2C^{\bullet}-OH$) and solvated protons ($(CH_3)_2CHOH_2^+$). In turn, the radical anions derived from a

DOI: 10.1021/acs.jpcb.8b01004
J. Phys. Chem. B 2018, 122, 4051−4066

solute can undergo protonation involving either the alcohol molecule and/or solvated protons.[50]

In the current study, we generated and identified radical ions and hydrogenated radicals derived from seven 3-styryl-quinoxalin-2-ones (3-SQ) (Chart 1) in acetonitrile and 2-propanol solutions, respectively.

Chart 1. Structures of 3-Styryl-quinoxalin-2(1*H*)-one (3-SQ) Derivatives under Study

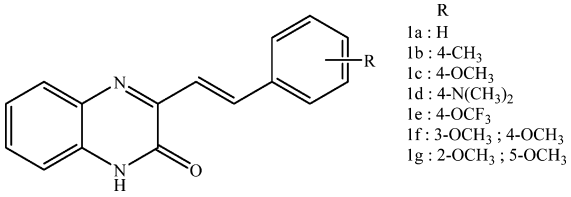

The insertion of a styryl moiety at the carbon atom (C3) should stabilize the C3 hydrogenated radical by the captodative effect of the N4 atom and C═O group in the pyrazine ring and by the resonance effect with the styryl moiety. This resonance could also facilitate the delocalization of the radical site over the sequence of double bonds and thus open the possibility for the formation of multiple stable products. Furthermore, the substitution in the para position either with electron-donating ($-CH_3$, $-OCH_3$, and $-N(CH_3)_2$) or with electron-withdrawing ($-OCF_3$) substituents in the styryl moiety (Chart 1, structures **1b**−**1e**) would modify the electronic distribution in the hydrogenated radical. Using seven 3-styryl-quinoxalin-2(1*H*)-one derivatives, one without substituents in the styryl moiety (Chart 1, structure **1a**), four others with electron-donating or electron-withdrawing substituents (Chart 1, structures **1b**−**1e**), and two with different double methoxy substituents (Chart 1, structures **1f**−**1g**), allowed for a detailed examination of substitution on the absorption maxima of the ensuing radical ions as well their stability.

The experimental spectra of the radical anions and hydrogenated radicals will be compared with the respective spectra calculated using ZINDO/S semiempirical quantum mechanical methods applied earlier for oxoisoaporphine and quinoxaline-2-one derivatives.[33,43,51] In turn, the experimental spectra of the radical cations will be compared with the respective spectra calculated using density functional theory (DFT).

EXPERIMENTAL SECTION

Materials. Acetonitrile was purchased from J.T. Baker with 99.95 purity (Baker HPLC analyzed), 2-propanol was purchased from Sigma-Aldrich with 99.8% purity (for HPLC), and they were used as received.

Synthesis of 3-Styryl-quinoxalin-2-ones (1a−g). Substituted 3-styryl-2(1*H*)-quinoxalin-2-ones (**1a**−**g**) were prepared by the thermic reaction of the corresponding benzaldehyde (3 mM) and 3-methyl-2(1*H*)-quinoxalin-2-one (1 mM) without solvents.[52] Both reagents were heated at 160 °C for 3 h under a nitrogen atmosphere in a pressure reactor vessel. After 3 h, the heating was stopped and the reactants were allowed to cool. The content of the flask was washed with a minimal amount of cold absolute ethanol/diethyl ether (1:1). The crude solid component was purified by column chromatography, eluted with dichloromethane/acetonitrile (9:1), and finally crystallized from acetonitrile, to give pure 3-styryl-quinoxalin-2-one derivatives.

High-Resolution Mass Spectrometry-Electrospray Ionization. High-resolution mass spectrometry-electrospray ionization (HRMS-ESI) spectra were obtained from a Thermo Fisher Scientific Exactive Plus mass spectrometer. The analysis for the reaction products was performed with the following relevant parameters: heater temperature, 50 °C; sheath gas flow, 5; sweep gas flow rate, 0; and spray voltage, 3.0 kV at the positive mode. Accurate mass measurements were performed at a resolution of 140.000.

Nuclear Magnetic Resonance. ^1H and ^{13}C nuclear magnetic resonance (NMR) spectra were obtained at 25 °C on a Bruker AVANCE 400 MHz spectrometer using tetramethylsilane as an internal standard. The NMR spectra were processed with MestReNova software v9.0. The spectral characterizations of **1a**−**g** by ^1H NMR and HRMS-ESI (+ mode) are in agreement with the expected structures. DMSO-d_6 ^1H and ^{13}C NMR data for the substrates are provided in the Supporting Information.

Preparation of Solutions. All solutions for pulse radiolysis experiments were prepared freshly before experiments with organic solvent and contained 0.1 mM 3-styryl-quinoxalin-2-one derivatives. Solutions were subsequently purged for at least 30 min per 200 mL of sample with the desired gas (Ar or O_2) before pulse irradiation.

Pulse Radiolysis. Pulse radiolysis experiments were performed with the INCT LAE 10 linear accelerator with a typical pulse duration of 7−10 ns and with the Notre Dame Titan 8 MeV Beta model TBS 8/16-1S with a typical pulse duration of 2−10 ns. Both data acquisition systems allow for kinetic traces to be displayed on multiple time scales. A detailed description of the experimental setups for optical measurements has been given elsewhere along with the basic details of the equipment and the data collection system.[53−55] The irradiation cells were supplied with a fresh solution by continuous and controlled flow of sample solutions at room temperature (~23 °C). Experimental error limits are ±10% unless specifically noted.

All experiments for substituted 3-styryl-2(1*H*)-quinoxalin-2-ones (**1a**−**g**) were performed on the pulse radiolysis setup coupled with the INCT LAE 10, whereas those for 3-methyl-2(1*H*)-quinoxalin-2-one were performed on the pulse radiolysis setup coupled with the Notre Dame Titan Beta model TBS 8/16-1S. The dose per pulse, which was determined by thiocyanate dosimetry, was on the order of 18−20 Gy with the INCT LAE 10 and 4−8 Gy for the Notre Dame Titan 8 MeV (1 Gy = 1 J kg^{-1}). Radiolytic yields are given in SI units as μmol J^{-1}, that is, the number of product species in micromoles that are generated for every joule of energy absorbed by the solution.

Quantum Mechanical Calculations. Semiempirical quantum mechanical calculations for radical anions (3-$SQ^{\bullet-}$) and their protonated forms (3-$SQH^{\bullet}$) were performed using HyperChem-8.03 by Hypercube, Inc. The structure geometries were optimized, and the respective formation enthalpies were calculated using the PM3 semiempirical method with the UHF approximation and the proper charge and multiplicity: −1 and 2 for the radical anions (3-$SQ^{\bullet-}$) and 0 and 2 for the protonated radical anions (3-$SQH^{\bullet}$). The structures of these latter species were constructed by adding the H atom in the proper position of the ground state of a 3-SQ molecule whose

DOI: 10.1021/acs.jpcb.8b01004
J. Phys. Chem. B 2018, 122, 4051−4066

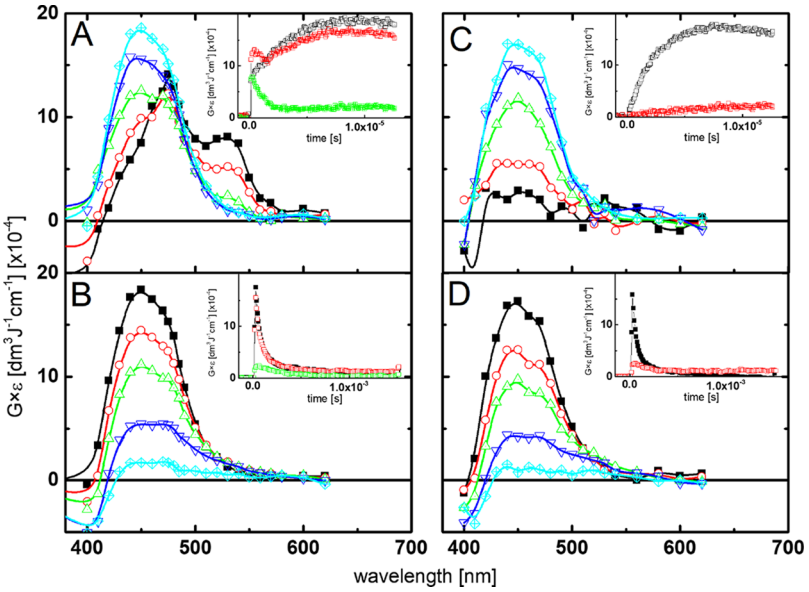

Figure 1. Absorption spectra recorded in Ar-saturated (A,B) acetonitrile solutions containing 0.1 mM 3-styryl-quinoxalin-2(1*H*)-one. Spectra were taken after the following time delays: (A) 240 ns (■), 800 ns (red circles), 2 μs (green up-pointing triangles), 4 μs (blue down-pointing triangles), and 8 μs (cyan diamonds) and inset: short-time profiles representing growth and/or decays at λ = 450 (□), 475 (red squares), and 530 nm (green squares); (B) 10 μs (■), 24 μs (red circles), 40 μs (green up-pointing triangles), 100 μs (blue down-pointing triangles), and 500 μs (cyan diamonds) and inset: long-time profiles representing decays at λ = 450 (■), 475 (red squares), and 530 nm (green squares). Absorption spectra recorded in O_2-saturated (C,D) acetonitrile solutions containing 0.1 mM 3-styryl-quinoxalin-2(1*H*)-one. Spectra were taken after the following time delays: (C) 240 ns (■), 800 ns (red circles), 2 μs (green up-pointing triangles), 4 μs (blue down-pointing triangles), 8 μs (cyan diamonds) and inset: short-time profiles representing growth at λ = 450 (□) and 530 nm (red squares); (D) 10 μs (■), 24 μs (red circles), 40 μs (green up-pointing triangles), 100 μs (blue down-pointing triangles), 500 μs (cyan diamonds) and inset: long-time profiles representing decays at λ = 450 (■) and 530 nm (red squares).

geometry was first optimized by the molecular mechanic method MM^+ followed by the PM3/UHF calculation. The respective spectra were calculated by using the ZINDO/S method applying the RHF approximation even for radical species. The first five unoccupied and five occupied molecular orbitals (MOs) with weighting factor values of 1.267 and 0.585 for $\sigma-\sigma$ and $\pi-\pi$ overlap were used for these calculations, respectively. By including more MOs (10 + 10), a greater number of absorption lines in the high-energy region were obtained, however, beyond the range of measurements performed. What is important, this inclusion did not affect the spectral region of interest in this study. All calculations were performed without taking into account any solvent effect that can likely shift the calculated absorption by a few nanometers.

All calculations for radical cations (3-$SQ^{\bullet+}$) were carried out employing M06-2x hybrid functional together[56] with the def2-TZVP basis set[57] for all atoms. Solvent effects were implicitly taken into account using COSMO[58] with ε = 37.5 for acetonitrile. Geometry optimizations were performed using an m5 grid to integrate the exchange and correlation contribution to the electronic energy. Vibrational normal modes were calculated to characterize nuclear configuration as a minimum in the potential energy surface (PES). Finally, time-dependent DFT (TDDFT) vertical excitation energies and oscillator strengths were obtained at the optimized ground state geometry at the M06-2x/def2-TZVP level of theory. All calculations were performed using TURBOMOLE software unless stated otherwise.[59] For selected radical cations, calculations were also carried out in vacuum employing CAM-B3LYP[60] and the same basis set to compare with M06-2x vertical excitations. These calculations were performed in NWChem.[61]

RESULTS

3-Styryl-quinoxalin-2(1*H*)-one (SQ (1a)). *Argon-Saturated Acetonitrile Solutions.* Pulse radiolysis of Ar-saturated acetonitrile solution containing 3-styryl-quinoxalin-2(1*H*)-one (**1a**, Chart 1) yielded a complex series of spectral changes (Figure 1A,B). A broad absorption was observed at 240 ns after the pulse in the 420−550 nm range, with two absorption maxima being located at λ_{max} = 475 and 530 nm with the respective $G\varepsilon_\lambda$ equal to 1.4×10^{-3} and 0.8×10^{-3} $dm^3\ J^{-1}\ cm^{-1}$ (Figure 1A). Both absorptions build up within <240 ns time domain; however, the growth at λ_{max} = 475 nm is more pronounced, and the transient absorption spectrum is dominated by the 475 nm band (Figure 1A). Moreover, the kinetic time profiles recorded at 475 and 530 nm are different (Figure 1A, inset). The absorption at 530 nm decayed further by a rapid first-order process with $k = 1.3 \times 10^6\ s^{-1}$ (inset in Figure 1A and Table 1). With the time elapsed when the 530 nm absorption band disappeared completely, the absorption spectrum underwent further changes, and 8 μs after the pulse is characterized by a broad and pronounced absorption band with λ_{max} = 450 nm with $G\varepsilon_{450}$ equal to 1.8×10^{-3} $dm^3\ J^{-1}\ cm^{-1}$ (Figure 1A). The growth of the 450 nm absorption band followed a first-order kinetics with $k = 3.9 \times 10^5\ s^{-1}$ (inset in Figure 1A).

However, to get the proper value for k of the growth measured at λ_{max} = 450 nm, a correction is needed because, in the first 5 μs after the pulse, the observed growth is perturbed by a concomitant simultaneous decay of the short-lived transient. Because the long-lived species does not absorb at λ = 550 nm, the observed decay at that wavelength was recorded and multiplied by a factor equal to the ratio of $G\varepsilon_{450}/G\varepsilon_{550}$ measured at 240 ns. The normalized decay was subtracted from

DOI: 10.1021/acs.jpcb.8b01004
J. Phys. Chem. B 2018, 122, 4051−4066

Table 1. Spectral Parameters of Radical Ions and Hydrogenated Radicals Derived from 3-Styryl-quinoxalin-2(1*H*)-one Derivatives (3-SQ) in Acetonitrile and 2-Propanol Solutions

compound 3-SQ	λ_{max} 3-SQ$^{\bullet-}$ (MeCN)	λ_{max} 3-SQ$^{\bullet+}$ (MeCN)	λ_{max} 3-SQ$^{\bullet-}$ (2-propanol)	λ_{max} 3-SQH$^{\bullet}$ (2-propanol)
SQ	475, 530	450	460, 520	480, 440[a]
4-CH_3SQ	470, 520	450–475	465, 520	480, 450[a]
4-OCH_3SQ	470, 510	485–490	470, 540	480, 450[a]
4-$N(CH_3)_2$SQ	490, 530	630	630	540
4-OCF_3SQ	475, 530	450	470, 520	490, 435
3,4-$(OCH_3)_2$SQ	470, 510	510	470, 520	480, 460[a]
2,5-$(OCH_3)_2$SQ	490, 540	490	475, 540	490, 470[a]

[a]Shoulder.

the recorded growth at λ = 450 nm (Figure 2). After correction, the growth of the 450 nm absorption band followed a first-order kinetics with $k = 3.9 \times 10^5$ s^{-1}.

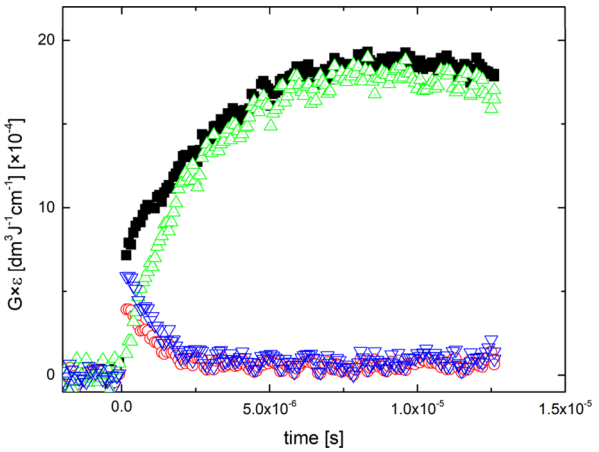

Figure 2. Kinetic traces recorded in Ar-saturated acetonitrile solutions containing 0.1 mM 3-styryl-quinoxalin-2(1*H*)-one (SQ) at λ = 550 nm (red circles) and 450 nm (■). The normalized decay (blue down-pointing triangles) and the corrected growth at λ = 450 nm (green up-pointing triangles) using the procedure described above in the text.

This absorption band was still observed at longer times, however, at 500 μs after the pulse was close to the completion (Figure 1B). The decay of the 450 nm band followed a rather more complex kinetics, which can be described as two first-order processes with $k = 2.2 \times 10^4$ and 2.8×10^3 s^{-1} (inset in Figure 1B and Table 2). All of these observations taken together point out the existence of at least two different transients.

Oxygen-Saturated Acetonitrile Solutions. To sort out the possible contributions of individual radical anions/triplets and radical cations derived from SQ, an acetonitrile solution containing 3-styryl-quinoxalin-2(1*H*)-one (**1a**, Chart 1) was saturated with oxygen as the scavenger for solvated electrons (e_{solv}^-) and/or dimeric radical anions $(CH_3CN)_2^{\bullet-}$. In the presence of oxygen, the absorption spectra recorded at short times after the pulse reveal different features (Figure 1C) in comparison to the spectra recorded at the same time under anaerobic conditions (Figure 1A).

Formation of the absorption band with the maxima at λ_{max} = 475 and 530 nm was completely suppressed. Therefore, it is reasonable to assume tentatively that the 3-styryl-quinoxalin-2(1*H*)-one-derived radical anions (SQ$^{\bullet-}$) (Figure 1A and Table 1) are only responsible for the absorption bands suppressed. The contribution of 3-styryl-quinoxalin-2-(1*H*)-one-derived triplets (^{3}SQ*) can be rather discarded based on flash photolysis experiments, in which the band assigned to ^{3}SQ* is characterized by the absorption band with λ_{max} = 435 nm (manuscript is under preparation).

The formation of the 450 nm band is also fully developed within the range of 8 μs (Figure 1C), and the formation kinetics recorded at λ = 450 nm with $k = 4.0 \times 10^5$ s^{-1} (inset in Figure 1C) matches nearly the formation kinetics of the 450 nm band in Ar-saturated acetonitrile (after correction) (inset in Figure 1A). The absorption spectrum recorded at 8 μs after the pulse exhibits a strong and broad absorption band with a maximum located at λ_{max} = 450 nm with $G\varepsilon_{450}$ equal to 1.7×10^{-3} dm^3 J^{-1} cm^{-1} (Figure 1C). Because the intensity of that absorption band is not affected by the presence of O_2, it is reasonable to assign it to the radical cation derived from 3-styryl-quinoxalin-2(1*H*)-one (SQ$^{\bullet+}$) (Figure 1C and Table 1). With the time further elapsed, the spectrum observed after 40 μs after the pulse is still characterized by a similar 450 nm absorption band (Figure 1D). Interestingly, the spectra observed at longer times (100 and 500 μs) after the pulse are characterized by a very broad and flat absorption band in the range 440–470 nm without a clearly pronounced maximum. The spectral and kinetic parameters of its formation and decay are similar to those observed in Ar-saturated (Tables 1 and 2), suggesting that the same species present in both Ar- and O_2-saturated solutions. For instance, the decay kinetics observed at λ = 450 nm followed again a complex kinetics, which can be described again as two first-order processes with $k = 2.3 \times 10^4$ and 1.9×10^3 s^{-1} (inset in Figure 1D and Table 2), similar to those measured in Ar-saturated solutions. Interestingly,

Table 2. Kinetic Parameters for the Growth and Decay of Radical Anions and Cations Derived from 3-Styryl-quinoxalin-2(1*H*)-one Derivatives in Acetonitrile Solutions Saturated with Either Ar or O_2

compound (3-SQ)	radical cation (3-SQ$^{\bullet+}$) growth (O_2) ($\times 10^5$ s^{-1})	radical cation (3-SQ$^{\bullet+}$) growth (Ar) ($\times 10^5$ s^{-1})	radical anion (3-SQ$^{\bullet-}$) decay (Ar) ($\times 10^6$ s^{-1})	radical cation (3-SQ$^{\bullet+}$) decay (O_2) (s^{-1})	radical cation (3-SQ$^{\bullet+}$) decay (Ar) (s^{-1})
SQ	4.0	3.9	1.3	2.3×10^4, 1.9×10^3	2.2×10^4, 2.8×10^3
4-CH_3SQ	3.8	3.8	1.5	2.0×10^4, 2.2×10^3	1.9×10^4, 3.3×10^3
4-OCH_3SQ	4.1	3.8[a]		2.4×10^4, 2.8×10^3	2.0×10^4, 3.4×10^3
4-$N(CH_3)_2$SQ	4.7	4.6	1.2	3.5×10^4, 3.6×10^3	6.2×10^4, 1.4×10^4
4-OCF_3SQ	3.8	3.9	1.2	2.8×10^4, 6.6×10^3	2.0×10^4, 2.5×10^3
3,4-$(OCH_3)_2$SQ	2.7	3.6[a]		2.0×10^4, 2.9×10^3	1.6×10^4, 2.9×10^3
2,5-$(OCH_3)_2$SQ	3.9	5.0[a]		1.9×10^4, 2.7×10^3	2.4×10^4, 3.6×10^3

[a]Not corrected growth by the procedure described in the text and displayed in Figure 2.

DOI: 10.1021/acs.jpcb.8b01004
J. Phys. Chem. B 2018, 122, 4051–4066

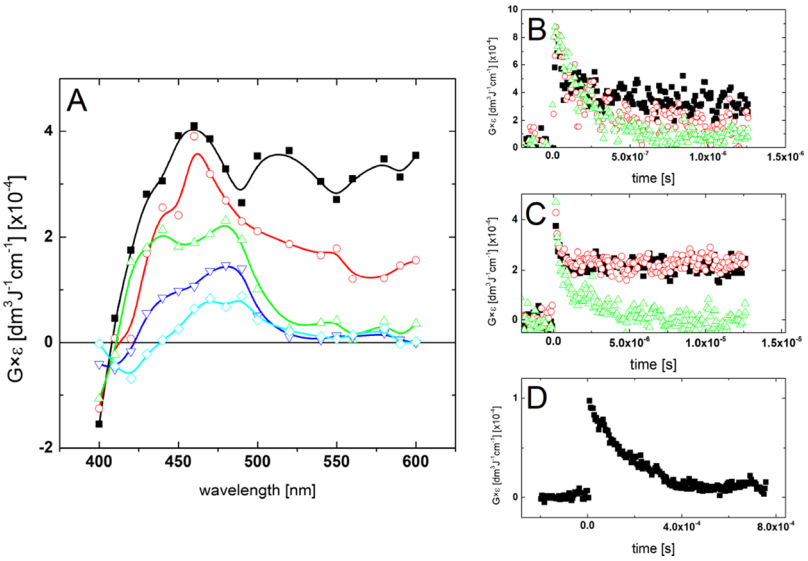

Figure 3. (A) Absorption spectra recorded in Ar-saturated 2-propanol solutions containing 0.1 mM 3-styryl-quinoxalin-2(1*H*)-one (SQ). Spectra were taken after the following time delays: 240 ns (■), 480 ns (red circles), 10 μs (green up-pointing triangles), 100 μs (blue down-pointing triangles), and 200 μs (cyan diamonds), (B) short-time profiles representing decays at λ = 460 (■), 520 (red circles), and 600 nm (green up-pointing triangles), (C) short-time profiles representing decays at λ = 440 (■), 480 (red circles), and 520 nm (green up-pointing triangles), and (D) long-time profile representing decay at λ = 480 (■).

comparison of the kinetic traces at λ = 450 and 530 nm clearly shows that, contrary to λ = 450 nm, the decay kinetics observed at λ = 530 nm follows a single first-order process with $k = 7.4 \times 10^3$ s^{-1} (inset in Figure 1D and Table 2). This last observation suggests the existence of two different cationic species. The assignment of the flat absorption band observed at longer times is not obvious, although very plausibly, it might be a dimeric radical cation ($(SQ)_2^{\bullet+}$) formed as a product of association of radical cations and parent SQ molecules. Formation of such species in stilbene[35] and styrene[62] derivatives is well-documented in the literature. However, taking into account the low concentration of SQ in the system studied, one can expect its very low yield.

Correction of the Absorption Spectrum of $SQ^{\bullet-}$. Subtraction of the absorption spectrum recorded 240 ns after the pulse in O_2-saturated solutions from the respective absorption spectrum obtained in Ar-saturated solutions should allow to take apart the contribution of radical cation ($SQ^{\bullet+}$), if any, leaving only the absorption spectrum that corresponds to the radical anion ($SQ^{\bullet-}$) at short times. Because the absorption signals recorded 240 ns after the pulse over the whole wavelength range (i.e., 400−600 nm) in O_2-saturated solutions are very weak (inset in Figure 1C) and being on the noise level, this clearly suggests that the absorption spectrum recorded at 240 ns after the pulse in Ar-saturated solutions can be assigned exclusively to radical anions ($SQ^{\bullet-}$) (Figure 1A and Table 1).

Ar-Saturated 2-Propanol Solutions. Pulse radiolysis of Ar-saturated 2-propanol solution containing 3-styryl-quinoxalin-2(1*H*)-one (**1a**, Chart 1) yielded a complex series of spectral changes. A broad absorption was observed at 240 ns after the pulse in the 420−600 nm range with two absorption maxima located at λ = 460 and 520 nm and with a rising absorption toward 600 nm with no defined maximum (Figure 3A).

This latter absorption can be assigned to the solvated electrons, which decay within the sub-microsecond time domain by a rapid pseudo-first-order process with $k = 5.5 \times 10^6$ s^{-1} (Table 3). At the time when the 600 nm absorption disappeared completely, the absorption bands with λ_{max} at 460 and 520 nm decreased also in intensity; however, the respective time profiles recorded at those wavelengths reached a plateau with a substantial offset (Figure 3B). The absorption spectrum observed 500 ns after the pulse is characterized by a distinct absorption maximum at λ_{max} = 460 nm and a pronounced shoulder located at 500−540 nm (Figure 3A).

Table 3. Kinetic Parameters for the Decays of Solvated Electrons (e_{solv}^-) and Radical Anions ($RSQ^{\bullet-}$) and Hydrogenated Radicals ($RSQH^{\bullet}$) Derived from 3-Styryl-quinoxalin-2(1*H*)-one Derivatives (3-SQ) in 2-Propanol Solutions Saturated with Ar

compound 3-SQ	solvated electron (e_{solv}^-) decay ($\times 10^6$ s^{-1})	radical anion ($3\text{-}SQ^{\bullet-}$) decay ($\times 10^5$ s^{-1})	hydrogenated radical ($3\text{-}SQH^{\bullet}$) decay ($\times 10^5 s^{-1}$)
SQ	5.5	5.0	6.4
4-CH_3SQ	6.1	7.1	3.7
4-OCH_3SQ	5.6	9.7	6.7
4-$N(CH_3)_2$SQ	6.4	4.6	8.6
4-OCF_3SQ	4.9	3.0	7.6
3,4-$(OCH_3)_2$SQ	5.5	5.6	6.2
2,5-$(OCH_3)_2$SQ	7.5	6.6	5.8

It is noteworthy that this absorption spectrum is very similar to the analogous spectrum recorded at 240 ns in Ar-saturated acetonitrile (Figure 1A), which was assigned to the 3-styryl-quinoxalin-2(1*H*)-one-derived radical anions ($SQ^{\bullet-}$). Moreover, the decays observed at λ_{max} = 460 and 520 nm look different (Figure 3C). At the time when 530 nm absorption disappeared in the pseudo-first order process with $k = 5.0 \times 10^5$ s^{-1} (Table 3), the spectrum underwent further changes, and 10 μs after the pulse is characterized by two distinct absorption maxima with λ_{max} at 440 and 480 nm (Figure 3A). Very plausibly, the decay observed at λ = 520 nm represents protonation of $SQ^{\bullet-}$ by the solvent (2-propanol) and the spectrum obtained can be tentatively assigned to the respective hydrogenated radical ($SQH^{\bullet}$). These two absorption bands are still observed at longer times (Figure 3A); however, at 100 and

DOI: 10.1021/acs.jpcb.8b01004
J. Phys. Chem. B 2018, 122, 4051−4066

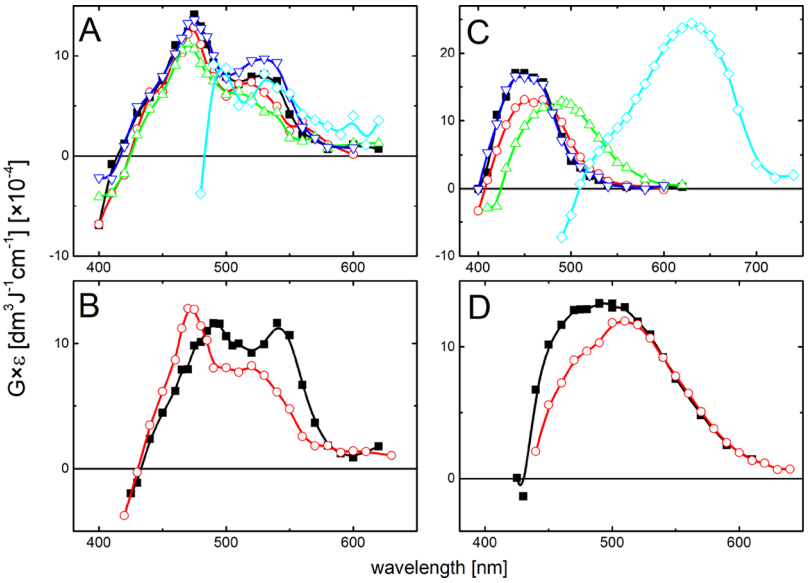

Figure 4. Absorption spectra recorded 240 ns after the pulse in Ar-saturated acetonitrile solutions containing 0.1 mM 3-styryl-quinoxalin-2(1*H*)-one derivatives with single substituents: (■) SQ, (red circles) 4-CH_3SQ, (green up-pointing triangles) 4-OCH_3SQ, (cyan diamonds) 4-$N(CH_3)_2$SQ, and (blue down-pointing triangles) 4-OCF_3SQ (A) and double methoxy substituents: (red circles) 3,4-$(OCH_3)_2$SQ and (■) 2,5-$(OCH_3)_2$SQ (B). Absorption spectra recorded 8 μs after the pulse in O_2-saturated acetonitrile solutions containing 0.1 mM 3-styryl-quinoxalin-2(1*H*)-one derivatives with single substituents: (■) SQ, (red circle) 4-CH_3SQ, (green up-pointing triangles) 4-OCH_3SQ, (cyan diamonds) 4-$N(CH_3)_2$SQ, and (blue down-pointing triangles) 4-OCF_3SQ (C) and double methoxy substituents: (red circles) 3,4-$(OCH_3)_2$SQ and (■) 2,5-$(OCH_3)_2$SQ (D).

200 μs after the pulse, the absorption band with a maximum at λ_{max} = 440 nm is transformed into a pronounced shoulder. The decay of the absorption band at λ_{max} = 480 nm (Figure 3D) occurs in the sub-millisecond time domain in a pseudo-first order process with $k = 6.4 \times 10^3$ s^{-1} (Table 3).

Argon- and Oxygen-Saturated Acetonitrile Solutions Containing 3-Styryl-quinoxalin-2-one Derivatives with Single Substituents. Because substitution in the para position by the electron-donating and electron-withdrawing groups does not affect significantly the time evolution of the spectral pattern and kinetic parameters of transients formed, both in Ar- and O_2-saturated acetonitrile solutions in comparison to SQ, discussions of the results will be limited to those parameters that were different and specific for the particular substituent.

3-(4-Methylstyryl)quinoxalin-2(1*H*)-one, 4-CH_3SQ (1b). Substitution in the para position by a weak electron-donating methyl group ($-CH_3$) ($\sigma_p = -0.17$)[63] in the styrene moiety affects slightly a transient absorption spectrum obtained 240 ns after the pulse in Ar-saturated solutions, which was assigned to radical anions (4-$CH_3SQ^{\bullet-}$) derived from 3-(4-methylstyryl)quinoxalin-2(1*H*)-one (4-CH_3SQ) based on the earlier assignment in SQ. The maxima of the respective absorption bands underwent a small hypsochromic shift of 5 and 10 nm and are located at λ = 470 and 520 nm with slightly lower $G\varepsilon_\lambda$ equal to 1.3×10^{-3} and 0.75×10^{-3} dm^3 J^{-1} cm^{-1}, respectively (Figures 4A and S1A in the Supporting Information and Table 1). The absorption at λ = 520 nm decayed by a rapid first-order process with $k = 1.5 \times 10^6$ s^{-1}, which is slightly higher than the analogous one in SQ (inset in Figure S1A in the Supporting Information and Table 2).

The absorption spectrum observed 8 μs after the pulse in both Ar- and O_2-saturated solutions is characterized by a broad and strong absorption band, however, with a weakly pronounced maximum located in the region 450−475 nm with $G\varepsilon_{450-475}$ ranged from 1.3×10^{-3} to 1.4×10^{-3} dm^3 J^{-1} cm^{-1} and was assigned to the radical cation ($MeSQ^{\bullet+}$) derived from 3-(4-methylstyryl)quinoxalin-2(1*H*)-one (MeSQ) (Figures 4A,C and S1A,C in the Supporting Information and Table 1).

The growth of the 450 nm absorption band followed a first-order kinetics with $k = 3.8 \times 10^5$ s^{-1} (after a similar correction for the simultaneous decay of the absorption at λ = 450 nm performed earlier for SQ) in Ar-saturated solutions, which matches nearly the formation kinetics in O_2-saturated solutions with $k = 3.7 \times 10^5$ s^{-1} (inset in Figure S1A in the Supporting Information and Table 2). Again, the decay of the 450 nm band, in both Ar- and O_2-saturated solutions, followed a complex kinetics, which can be described as two first-order processes, with the first-order *k*-values differing by the order of magnitude and which are also comparable to the respective *k*-values measured for SQ (insets in Figure S1B,D in the Supporting Information and Table 2).

3-(4-Methoxystyryl)quinoxalin-2(1*H*)-one, 4-OCH_3SQ (1c). Substitution in the para position by a stronger electron-donating methoxy group ($-OCH_3$) ($\sigma_p = -0.27$)[63] in the styrene moiety practically does not affect the spectral parameters of the radical anions (4-$OCH_3SQ^{\bullet-}$) derived from 3-(4-methoxystyryl)quinoxalin-2(1*H*)-one (4-OCH_3SQ), except for a further small hypsochromic shift of 20 nm of the second absorption band maximum to λ_{max} = 510 nm with respective $G\varepsilon_{470}$ equal to 1.2×10^{-3} dm^3 J^{-1} cm^{-1} and $G\varepsilon_{510} = 0.65 \times 10^{-3}$ dm^3 J^{-1} cm^{-1} (Figures 4A and S2A in the Supporting Information and Table 1), as compared to SQ. Contrary to SQ and 4-CH_3SQ, the fast decay of the second absorption band at λ_{max} = 510 nm of 4-$OCH_3SQ^{\bullet-}$ is not observed because of the overlap with a slower growth of a broad and strong absorption band with a weakly pronounced maximum at λ_{max} = 485 nm and $G\varepsilon_{485}$ equal to 1.2×10^{-3} dm^3 J^{-1} cm^{-1} (inset in Figure S2A in the Supporting Information and Table 1). Therefore, it is not possible to extract in a straightforward way the rate constant (*k*) of this fast first-order decay. This band is also present in O_2-saturated solutions with

DOI: 10.1021/acs.jpcb.8b01004
J. Phys. Chem. B 2018, 122, 4051−4066

no clearly visible maximum located at λ_{max} = 485−490 nm with $G\varepsilon_{490}$ equal to 1.3 × 10^{-3} dm^3 J^{-1} cm^{-1} (Figures 4C and S2C in the Supporting Information and Table 1). The growth of that band assigned to radical cations (4-$OCH_3SQ^{\bullet+}$) derived from 3-(4-methoxystyryl)quinoxalin-2(1*H*)-one (4-OCH_3SQ) followed a first-order kinetics with k = 3.8 × 10^5 s^{-1} (in Ar-saturated solutions) (inset in Figure S2A in the Supporting Information) and k = 4.1 × 10^5 s^{-1} (in O_2-saturated solutions) (inset in Figure S2C in the Supporting Information), which are very close to those measured for SQ and 4-CH_3SQ (Table 2). Similarly to $SQ^{\bullet+}$ and 4-$CH_3SQ^{\bullet+}$, the decay of 4-$OCH_3SQ^{\bullet+}$ in both Ar- and O_2-saturated solutions followed a complex kinetics described again as two first-order processes, with the first-order k-values differing by the order of magnitude (insets in Figure S2B,D in the Supporting Information and Table 2), which are also comparable to the respective k-values measured for $SQ^{\bullet+}$ and 4-$CH_3SQ^{\bullet+}$ (Table 2).

3-(4-*N*,*N*-Dimethylaminestyryl)quinoxalin-2(1*H*)-one, 4-N$(CH_3)_2$SQ (1d). Substitution in the para position by a strong electron-donating dimethylamine group (−N$(CH_3)_2$) (σ_p = −0.83)[63] in the styrene moiety does not affect much the spectral and kinetic parameters of the radical anions (4-N$(CH_3)_2SQ^{\bullet-}$) derived from 3-(4-*N*,*N*-dimethylstyryl)-quinoxalin-2(1*H*)-one (4-N$(CH_3)_2$SQ), except for a small bathochromic shift of 15 nm of the first absorption band maximum to λ_{max} = 490 nm with the respective $G\varepsilon_{490}$ = 0.9 × 10^{-3} dm^3 J^{-1} cm^{-1} and $G\varepsilon_{530}$ = 0.8 × 10^{-3} dm^3 J^{-1} cm^{-1} (at λ = 530 nm), as compared to $SQ^{\bullet-}$ (Figures 4A and S3A in the Supporting Information and Table 1). Both absorption bands decayed by a rapid first-order process with k = 1.2 × 10^6 s^{-1} (measured at λ = 490 nm), which is slightly lower than the analogous one for SQ (inset in Figure S3A in the Supporting Information and Table 2). On the other hand, the substitution affects substantially the spectral parameters of the long-lived transient, in both Ar- and O_2-saturated solutions, which is assigned to the radical cations (4-N$(CH_3)_2SQ^{\bullet+}$) derived from 3-(4-*N*,*N*-dimethylstyryl)quinoxalin-2(1*H*)-one (4-N$(CH_3)_2$SQ) (Figures 4A,C and S3A,C in the Supporting Information and Table 1). The maximum of the absorption band of 4-N$(CH_3)_2SQ^{\bullet+}$ underwent a significant bathochromic shift to λ = 630 nm as compared to $SQ^{\bullet+}$ with $G\varepsilon_{630}$ equal to 1.9 × 10^{-3} dm^3 J^{-1} cm^{-1} (in Ar-saturated solutions) (Figure 4A) and 2.2 × 10^{-3} dm^3 J^{-1} cm^{-1} (in O_2-saturated solutions) (Figure 4C and Table 1). The growth of the 630 nm absorption band followed a first-order kinetics with k = 4.6 × 10^5 s^{-1} (in Ar-saturated solutions) (inset in Figure S3A in the Supporting Information and Table 2) and k = 4.7 × 10^5 s^{-1} (in O_2-saturated solutions) (inset in Figure S3C in the Supporting Information and Table 2), which are slightly higher than those measured for other SQ derivatives (Table 2). Similarly to $SQ^{\bullet+}$, 4-$CH_3SQ^{\bullet+}$, and 4-$OCH_3SQ^{\bullet+}$, the decay of 4-N$(CH_3)_2SQ^{\bullet+}$ in both Ar- and O_2-saturated solutions followed a complex kinetics described again as two first-order processes, with the first-order k-values differing by the order of magnitude (insets in Figure S3B,D and Table 2), which are also comparable to the respective k-values measured for $SQ^{\bullet+}$, 4-$CH_3SQ^{\bullet+}$, and 4-$OCH_3SQ^{\bullet+}$ (Table 2).

3-(4-Trifluoromethoxystyryl)quinoxalin-2(1*H*)-one, 4-OCF_3SQ (1e). Substitution in the para position by a relatively strong electron-withdrawing trifluoromethoxy group (−OCF_3) (σ_p = +0.35)[63] does not affect at all the time evolution of the spectral pattern and kinetic parameters of transients formed in both Ar- and O_2-saturated solutions in comparison to SQ.

In Ar-saturated solutions, the short-lived species is formed within 240 ns time domain and is characterized by the spectrum with two absorption bands located at λ_{max} = 475 and 530 nm with the respective $G\varepsilon_{475}$ = 1.4 × 10^{-3} dm^3 J^{-1} cm^{-1} and $G\varepsilon_{530}$ = 1.0 × 10^{-3} dm^3 J^{-1} cm^{-1} (Figures 4A and S4A in the Supporting Information and Table 1). Similarly, as for the other derivatives, this absorption spectrum is assigned to the radical anions (4-$OCF_3SQ^{\bullet-}$) derived from 3-(4-trifluoromethoxystyryl)quinoxalin-2(1*H*)-one (4-OCF_3SQ) (Table 1). 4-$OCF_3SQ^{\bullet-}$ decayed by a rapid first-order process with k = 1.2 × 10^6 s^{-1} (inset in Figure S4A in the Supporting Information and Table 2). The absorption spectrum underwent further changes, and 8 μs after the pulse is characterized by a broad and pronounced absorption band with λ_{max} = 450 nm, in both Ar- (Figures 4A and S4A in the Supporting Information) and O_2-saturated solutions (Figures 4C and S4C in the Supporting Information and Table 1). This absorption band, in analogy to other SQ derivatives, has been assigned to the radical cations (4-$OCF_3SQ^{\bullet+}$) derived from 3-(4-trifluoromethoxy-styryl)quinoxalin-2(1*H*)-one (4-OCF_3SQ) (Table 1). The growth of the 450 nm absorption band followed a first-order kinetics with k = 3.9 × 10^5 s^{-1} (in Ar-saturated solutions) (inset in Figure S4A in the Supporting Information and Table 2) and k = 3.8 × 10^5 s^{-1} (in O_2-saturated solutions) (inset in Figure S4C in the Supporting Information and Table 2), which are similar to those measured for other SQ derivatives (Table 2). The decay of 4-$OCF_3SQ^{\bullet+}$ in both Ar- and O_2-saturated solutions followed a complex kinetics described again as two first-order processes, with the first-order k-values differing by the order of magnitude (insets in Figure S4B,D and Table 2), which are also comparable to the respective k-values measured earlier for other 3-$SQ^{\bullet+}$ radical cations with a single substituent (Table 2).

Argon-Saturated 2-Propanol Solutions Containing 3-Styryl-quinoxalin-2(1H)-one Derivatives with Single Substituents. Because substitution in the para position by the electron-donating and electron-withdrawing groups does not affect significantly the time evolution of the spectral pattern and kinetic parameters of transients formed in Ar-saturated 2-propanol solutions in comparison to SQ (except for **1d**), the respective spectra and short- and long-time profiles at selected wavelengths are presented in the Supporting Information (Figures S7−S10). Similar to SQ (**1a**), pulse radiolysis of Ar-saturated 2-propanol solutions containing 3-styryl-quinoxalin-2(1*H*)-one derivatives (**1b**−**1e**) with methyl (CH_3−) (**1b**), methoxy (−OCH_3) (**1c**), *N*,*N*-dimethylamine (−N$(CH_3)_2$) (**1d**), and trifluoromethoxy (−OCF_3) (**1e**) groups yielded a complex series of spectral changes. The spectra observed in the sub-microsecond time domain can be assigned to the respective radical anions (3-$SQ^{\bullet-}$), and those observed in the microsecond time domain can be assigned to the respective hydrogenated radicals (3-$SQH^{\bullet}$). It is noteworthy that the spectral parameters of radical anions (3-$SQ^{\bullet-}$) derived from 3-(styryl)quinoxalin-2(1*H*)-one derivatives (**1b**, **1c**, and **1e**) match very well the spectral parameters of 3-$SQ^{\bullet-}$ observed in acetonitrile solutions (Table 1). The only exception is **1d**, where the maximum of the absorption band of 4-N$(CH_3)_2SQ^{\bullet-}$ underwent a significant bathochromic shift to λ = 630 nm (Figure S9 in the Supporting Information) as compared to λ_{max} = 490 and 530 nm observed in acetonitrile solutions (Table 1). On the other hand, the hydrogenated radicals (3-$SQH^{\bullet}$), which were not observed in acetonitrile solutions, are characterized by the absorption spectra with λ_{max}

DOI: 10.1021/acs.jpcb.8b01004
J. Phys. Chem. B 2018, 122, 4051−4066

= 480−490 nm, depending on the substituent (Table 1). Again, the only exception is **1d**, where the maximum of the absorption band of 4-N$(CH_3)_2$SQH$^•$ underwent a bathochromic shift to λ = 550 nm (Figure S9 in the Supporting Information). The rate constants of the respective processes occurring for 3-(styryl)-quinoxalin-2(1*H*)-one derivatives (3-SQ) (**1b**−**1e**), which were described in detail for SQ (**1a**), are collected in Table 3.

Argon- and Oxygen-Saturated Acetonitrile Solutions Containing 3-Styryl-quinoxalin-2(1H)-one Derivatives with Double Methoxy Substituents. Because simultaneous substitution in the para/meta and ortho/meta positions by relatively strong electron-donating methoxy groups does not affect significantly the time evolution of the spectral pattern and kinetic parameters of transients formed, in both Ar- and O_2-saturated acetonitrile solutions in comparison to a single-substituted methoxy 3-styryl-quinoxalin-2-one derivative (4-OCH_3SQ), discussions of the results will be limited to those parameters that were different and specific for the particular combination of substitutions.

3-(3,4-Dimethoxystyryl)quinoxalin-2(1*H*)-one, 3,4-$(OCH_3)_2$SQ (1f). Substitution in the para and meta positions by two electron-donating methoxy groups (−OCH_3) (σ_p = −0.27)[63] in the styrene moiety practically does not affect the spectral parameters of the radical anions (3,4-$(OCH_3)_2SQ^{•−}$) derived from 3-(3,4-dimethoxystyryl)quinoxalin-2(1*H*)-one (3,4-$(OCH_3)_2$SQ), with $G\varepsilon_{470}$ equal to 1.3 × 10^{-3} dm^3 J^{-1} cm^{-1} and $G\varepsilon_{510}$ to 0.8 × 10^{-3} dm^3 J^{-1} cm^{-1} (Figures 4B and S5A in the Supporting Information and Table 1), as compared to 4-OCH_3SQ (Figures 4A and S2A and Table 1). Similar to 4-OCH_3SQ, however, contrary to SQ and other SQ derivatives, the fast decay of the second absorption band at λ_{max} = 510 nm of 3,4-$(OCH_3)_2SQ^{•−}$ is not observed because of the overlap with a slower growth of a broad and strong absorption band with a weakly pronounced maximum at λ_{max} = 510 nm and $G\varepsilon_{510}$ equal to 1.3 × 10^{-3} dm^3 J^{-1} cm^{-1} (inset in Figure S5A in the Supporting Information and Table 1). Therefore, it is not possible to extract in a straightforward way the rate constant (k) of this fast first-order decay. The growth of that band assigned to radical cations (3,4-$(OCH_3)_2SQ^{•+}$) derived from 3-(3,4-dimethoxystyryl)quinoxalin-2(1*H*)-one (3,4-$(OCH_3)_2$SQ) followed a first-order kinetics with k = 3.6 × 10^5 s^{-1} (in Ar-saturated solutions) (inset in Figure S5A in the Supporting Information and Table 2) and k = 2.7 × 10^5 s^{-1} (in O_2-saturated solutions) (inset in Figure S5C in the Supporting Information and Table 2). These rate constants differ slightly, which is due to the fact that the growth recorded at λ = 510 nm in Ar-saturated solutions and assigned to the formation of 3,4-$(OCH_3)_2SQ^{•+}$ was not corrected by the simultaneous decay of 3,4-$(OCH_3)_2SQ^{•−}$. The decay of 3,4-$(OCH_3)_2SQ^{•+}$ in both Ar- and O_2-saturated solutions followed a complex kinetics described again as two first-order processes, with the first-order k-values differing by the order of magnitude (insets in Figure S5B,D in the Supporting Information and Table 2), which are also comparable to the respective k-values measured earlier for other 3-$SQ^{•+}$ radical cations with single substituents (Table 2).

3-(2,5-Dimethoxystyryl)quinoxalin-2(1*H*)-one, 2,5-MeOSQ (1g). Substitution in the ortho and meta positions by two electron-donating methoxy groups (−OCH_3) (σ_p = −0.27)[63] in the styrene moiety affects slightly the spectral parameters of the radical anions (2,5-$(OCH_3)_2SQ^{•−}$) derived from 3-(2,5-dimethoxystyryl)quinoxalin-2(1*H*)-one (2,5-$(OCH_3)_2$SQ), with $G\varepsilon_{490}$ equal to 1.2 × 10^{-3} dm^3 J^{-1} cm^{-1} and $G\varepsilon_{540}$ to 1.2 × 10^{-3} dm^3 J^{-1} cm^{-1} (Figures 4B and S6A in the Supporting Information and Table 1) as compared to 4-OCH_3SQ and 3,4-$(OCH_3)_2$SQ (Figure 4B and Table 1). Similarly to 4-OCH_3SQ and 3,4-$(OCH_3)_2$SQ, the fast decay of the second absorption band at λ_{max} = 540 nm of 2,5-$(OCH_3)_2SQ^{•−}$ is not observed because of the overlap with a slower growth of a broad and strong absorption band with a weakly pronounced maximum at λ_{max} = 490 nm and $G\varepsilon_{490}$ equal to 1.4 × 10^{-3} dm^3 J^{-1} cm^{-1} (inset in Figure S6A in the Supporting Information and Table 1). Therefore, it was not possible to extract again in a straightforward way the rate constant (k) of this fast first-order decay. The growth of that band assigned to radical cations (2,5-$(OCH_3)_2SQ^{•+}$) derived from 3-(2,5-dimethoxystyryl)quinoxalin-2(1*H*)-one (2,5-$(OCH_3)_2$SQ) followed a first-order kinetics with k = 5.0 × 10^5 s^{-1} (in Ar-saturated solutions) (inset in Figure S6A in the Supporting Information and Table 2) and k = 3.9 × 10^5 s^{-1} (in O_2-saturated solutions) (inset in Figure S6C in the Supporting Information and Table 2). The decay of 2,5-$(OCH_3)_2SQ^{•+}$ in both Ar- and O_2-saturated solutions followed a complex kinetics described again as two first-order processes, with the first-order k-values differing by the order of magnitude (insets in Figure S6B,D in the Supporting Information and Table 2), which are also comparable to the respective k-values measured earlier for 3,4-$(OCH_3)_2SQ^{•+}$ and the other 3-$SQ^{•+}$ radical cations with single substituents (Table 2).

Argon-Saturated 2-Propanol Solutions Containing 3-Styryl-quinoxalin-2(1H)-one Derivatives with Double Methoxy Substituents. Because substitution in the para/meta and ortho/meta positions with double methoxy substituents does not affect significantly the time evolution of the spectral pattern and kinetic parameters of transients formed in Ar-saturated 2-propanol solutions in comparison to SQ, the respective spectra and short- and long-time profiles at selected wavelengths are also presented in the Supporting Information (Figures S11 and S12). Similar to SQ (**1a**), pulse radiolysis of Ar-saturated 2-propanol solutions containing 3-styryl-quinoxalin-2(1*H*)-one derivatives (**1f**−**1g**) with methoxy (−OCH_3) groups in the para/meta positions (**1f**) and the ortho/meta positions (**1g**) yielded also a complex series of spectral changes. Again, the spectra observed in the sub-microsecond time domain can be assigned to the respective radical anions (3-$SQ^{•−}$), and those observed in the microsecond time domain can be assigned to the respective hydrogenated radicals (3-$SQH^•$). It is noteworthy that the spectral parameters of radical anions (3-$SQ^{•−}$) derived from 3-(styryl)quinoxalin-2(1*H*)-one derivatives (**1f**−**1g**) match very well the spectral parameters of 3-$SQ^{•−}$ observed in acetonitrile solutions (Table 1). The respective hydrogenated radicals (3-$SQH^•$), which were not observed in acetonitrile solutions, are characterized by the absorption spectra located in the range of 420−520 nm with a maximum located at λ = 480−490 nm, depending on the location of methoxy substituents (Table 1). The rate constants of the respective processes occurring for 3-(styryl)quinoxalin-2(1*H*)-one derivatives (3-SQ) (**1f**−**1g**), which were described in detail for SQ (**1a**), are collected in Table 3.

Argon- and Oxygen-Saturated Acetonitrile Solutions Containing 3-Methyl-quinoxalin-2(1H)-one (3-MeQ). For the sake of the later discussion, reference spectra for radical cations and anions derived from the compound containing a quinoxaline-2-one moiety without a styryl substituent in position 3, Ar- and O_2-saturated acetonitrile solutions containing 3-methyl-quinoxalin-2-one (3-MeQ) were generated

DOI: 10.1021/acs.jpcb.8b01004
J. Phys. Chem. B 2018, 122, 4051−4066

by pulse radiolysis. This information is important to check to what extent replacement of a methyl group by a styryl moiety at carbon 3 influences the spectral characteristics of the transients formed.

A transient absorption spectrum obtained 600 ns after the electron pulse in Ar-saturated solutions exhibited a distinct absorption band with λ_{max} = 425 nm with $G\varepsilon_{425}$ equal to 8.5 × 10^{-4} dm^3 J^{-1} cm^{-1} (Figure S13 in the Supporting Information). The decay kinetic trace showed a decay (inset in Figure S13 in the Supporting Information), which is nearly completed after 50 μs after the pulse (Figure S13 in the Supporting Information). Interestingly, absorption spectrum 6 μs after the pulse is characterized by a new pronounced absorption band with λ_{max} = 375 nm with $G\varepsilon_{375}$ equal to 8.5 × 10^{-4} dm^3 J^{-1} cm^{-1} (Figure S13 in the Supporting Information). At this point in the exposition, we will not attempt to assign unambiguously the species responsible for the 375 and 425 nm absorption bands; however, considering the character of primary species present in Ar-saturated acetonitrile solutions, one can presumably claim that the radical ions (3-MeQ$^{\bullet+}$ and 3-MeQ$^{\bullet-}$) derived from 3-MeQ are responsible for the presence of these two bands. To solve this issue, the transient absorption spectra were recorded in irradiated O_2-saturated acetonitrile solutions containing 3-MeQ. Contrary to Ar-saturated solutions, the transient absorption spectrum recorded 600 ns after electron pulse does not reveal the 425 nm absorption band, only a weak absorption band with λ_{max} = 375 nm (Figure S14 in the Supporting Information). This absorption reaches the maximum 6 μs after the pulse (similar to in Ar-saturated solutions) with $G\varepsilon_{375}$ equal to 4.5 × 10^{-4} dm^3 J^{-1} cm^{-1}. All of these observations taken together clearly show the existence of two different radical ions derived from 3-MeQ, radical cations (3-MeQ$^{\bullet+}$) and radical anions (3-MeQ$^{\bullet-}$) characterized by absorption bands with λ_{max} = 375 nm and λ_{max} = 425 nm, respectively.

Semiempirical and DFT Quantum Mechanics Calculations. Radical Anions (3-SQ$^{\bullet-}$). Semiempirical calculations of electronic transitions described in the Experimental Section gave fairly good agreement with the experimentally measured electronic transitions in the maxima for all 3-SQ$^{\bullet-}$ radical anions (Table 1). The transitions showing the largest values of oscillator strength for 3-SQ$^{\bullet-}$ radical anions are presented in Table 4.

It is noteworthy that the experimental absorption spectra characterized by two absorption maxima at $\lambda \approx 470$ nm and at λ = 520 nm are reproduced adequately with a difference between calculated and experimental values smaller than 0.1 eV, irrespective of the solvent considered, acetonitrile or 2-propanol (see Table 1).

On the other hand, semiempirical calculations of electronic transitions for all 3-SQ$^{\bullet+}$ radical cations failed in reproducing the experimentally observed absorption maxima. Therefore, the more sophisticated methodology was used (vide supra in Quantum Mechanical Calculations).

Protonated Radical Anions (Hydrogenated Radicals) (3-SQH$^{\bullet}$). Radical anions derived from 3-styryl-quinoxalin-2-one derivatives (3-SQ$^{\bullet-}$) have at least four sites at which they might be protonated, forming the respective neutral protonated radicals: (i) at N4 of quinoxaline-2-one giving 3-SQNH$^{\bullet}$ radical, which should be stabilized by a captodative and resonance effect, (ii) at the carbonyl oxygen, 3-SQOH$^{\bullet}$ radical, and (iii) at two carbon atoms located in the vinyl bond 3-SQC11H$^{\bullet}$ (where C11 is the C-atom directly bound to the quinoxaline-2-one moiety) and 3-SQC12H$^{\bullet}$ (where C12 is the C-atom directly bound to the benzene moiety). The calculated formation enthalpies for these hydrogenated radicals confirm that the most stable neutral radicals (3-SQH$^{\bullet}$) are those obtained by the protonation of 3-SQ$^{\bullet-}$ radical anions at N4-atom (Table S1 in the Supporting Information). Unfortunately, the calculated spectra, PM3-ZINDO/S (data not shown), for these species failed in reproducing the experimental absorption maxima attributed to the hydrogenated radicals generated by pulse radiolysis in 2-propanol.

Radical Cations (3-SQ$^{\bullet+}$). The first 10 vertical excitation energies together with oscillator strengths (f_{max}) and spin contaminations for the radical cations derived from seven 3-styryl-quinoxalin-2-one derivatives studied are collected in Tables S2 and S3 (Supporting Information). It is worthy to note that the spin contamination $\langle S^2 \rangle$ is small, about 5% for all radical cations. Those transitions showing the largest values of the oscillator strength are presented in Table 5.

Table 4. Calculated Spectral Parameters of Radical Anions (3-SQ$^{\bullet-}$) Derived from 3-Styryl-quinoxalin-2(1*H*)-one Derivatives (3-SQ)

radical anions 3-SQ$^{\bullet-}$	λ_{max}	f_{max}[a]
SQ$^{\bullet-}$	446.9, 526.8	1.033, 0.120
4-CH_3SQ$^{\bullet-}$	485.5, 555.8	0.756, 0.121
4-OCH_3SQ$^{\bullet-}$	448.0, 526.1	1.028, 0.130
4-N$(CH_3)_2$SQ$^{\bullet-}$	471.4, 475.8, 550.8	0.261, 0.685, 0.126
4-OCF_3SQ$^{\bullet-}$	490.4, 552.0	0.678, 0.237
3,4-$(OCH_3)_2$SQ$^{\bullet-}$	445.7, 449.6, 521.7	0.793, 0.242, 0.148
2,5-$(OCH_3)_2$SQ$^{\bullet-}$	481.6, 549.2	0.698, 0.194

[a]Only displayed oscillator strengths larger than 0.1.

DISCUSSION

The present work reports for the first time on spectral data regarding the radical anions and radical cations derived from seven 3-styryl-quinoxalin-2-one derivatives. In addition, the kinetics of formation and decay of these transients were presented and the respective rate constants were measured.

Radical Anions (3-SQ$^{\bullet-}$). The observed absorption spectra in Ar-saturated acetonitrile solutions and assigned to the radical anions of 3-styryl-quinoxalin-2-one derivatives (3-SQ$^{\bullet-}$) are characterized by two absorption maxima: the first one is clearly pronounced and located in the range of 470−490 nm and the second one is located in the range of 510−540 nm, less intensive, and less pronounced (Table 1). They are in general agreement with the results of the ZINDO/S semiempirical quantum mechanical calculations (Table 4). It has to be noted that the substituents in the benzene ring influence slightly the position of the absorption band by shifting its maximum to the shorter wavelength (λ_{max} = 470 nm) for the methyl, and methoxy groups at position 4 in the benzene ring for single-substituted derivatives, and methoxy groups at positions 3 and 4 in the benzene ring for double-substituted derivatives as compared with that observed for the nonsubstituted 3-styryl-quinoxalin-2-one derivative. This might suggest a partial delocalization of the negative charge into the aromatic ring. Interestingly, there is no change in spectral parameters for the triflurometoxy group (an electron-withdrawing group) at position 4. The most noticeable shifts in λ_{max} to 490 nm were observed for the dimethylamine group at position 4 for single-

DOI: 10.1021/acs.jpcb.8b01004
J. Phys. Chem. B 2018, 122, 4051−4066

Table 5. Calculated Spectral Parameters of Radical Cations Derived from 3-Styryl-quinoxalin-2(1*H*)-one Derivatives (4R-3SQ) Employing M06-2x Hybrid Functional with def2-TZVP Basis Set

radical cation 3-SQ$^{\bullet+}$	number of a vertical transition	λ_{max}	f_{max} [a]	w [b]
SQ$^{\bullet+}$	S5	452	0.867	$H_\alpha \rightarrow L_\alpha$ (85)
4-CH_3SQ$^{\bullet+}$	S5	457	0.934	$H_\alpha \rightarrow L_\alpha$ (84)
4-OCH_3SQ$^{\bullet+}$	S5	450	0.865	$H_\alpha \rightarrow L_\alpha$ (73)
4-N$(CH_3)_2$SQ$^{\bullet+}$	S4	440, 679 [c]	0.670, 0.339	$H_\alpha \rightarrow L_\alpha$ (56), $H_\beta \rightarrow L_\beta$ (65)
4-OCF_3SQ$^{\bullet+}$	S5	457	0.930	$H_\alpha \rightarrow L_\alpha$ (85)
3,4-$(OCH_3)_2$SQ$^{\bullet+}$	S4	444	0.458	$H_\alpha \rightarrow L_\alpha$ (52)
2,5-$(OCH_3)_2$SQ$^{\bullet+}$	S8	340	0.596	$H_\beta \rightarrow L{+}1_\beta$ (41), $H_\alpha \rightarrow L_\alpha$ (34)

[a]Oscillator strengths. [b]Main MO contributions for the transitions with the largest oscillator strength. [c]The transition with the second largest value of the oscillator strength.

substituted derivatives and for methoxy groups at positions 2 and 5 for double-substituted derivatives. Indeed, the locations of wavelength maxima of radical anions are not affected as much as radical cations in acetonitrile solvents and do not follow so clearly an order based on inductive and resonance effects (Table 1). Generally, it is well-known that electron-withdrawing groups lower the energy of a MO, whereas electron-donating groups increase it. The most noticeable bathochromic shift in λ_{max} (20 nm) to 490 nm was observed for the $-N(CH_3)_2$ group at position 4, which is an electron-donating group, because of both inductive and resonance effects. Therefore, this behavior seems to be reasonable because the electron-donating group adds electron density to the π-system, thus increasing significantly the energy of an MO. Interestingly, there is no change in λ_{max} for $-OCF_3$ group at position 4 which is electron withdrawing by inductive effect but electron donating by resonance effect and surprisingly also for $-OCH_3$ which is electron-donating group due to both inductive and resonance effects. As far as the doubly $-OCH_3$ substituted derivatives are concerned, for 2,5-$(OCH_3)_2$-SQ, only inductive electron donor effect is expected but, for 3,4-$(OCH_3)_2$-SQ, both inductive and resonance electron donor effects are expected. The observation that 2,5-$(OCH_3)_2$-SQ possesses a 20 nm red shift relative to 3,4-$(OCH_3)_2$-SQ might suggest a larger contribution of the inductive effect over the resonance effect. Moreover, the inductive and resonance effects should push the charge to the quinoxaline-2-one moiety, and likely the electronic transitions observed for the radical anions are dominated by those located in that moiety. Because the substitution occurs at the peripheral positions of the quinoxaline-2-one ring, this cannot affect much the spectroscopic properties of these species.

Similar spectral features of 3-SQ$^{\bullet-}$ were observed in Ar-saturated 2-propanol solutions, that is, a first absorption maximum located in the range of 460−475 nm and a second maximum, less intensive, located in the range of 520−540 nm.

The radical anions can be formed either by a direct attachment of the solvated electrons (e_{solv}^-) formed in acetonitrile and 2-PrOH to 3-SQ or by an electron transfer from $CH_3CN^{\bullet-}$, $(CH_3CN)_2^{\bullet-}$, or $(CH_3)_2C^{\bullet}$-OH to 3-SQ in acetonitrile and 2-PrOH, respectively (reaction 1):

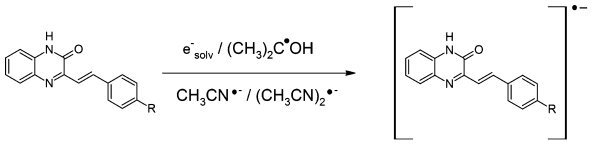

Generally, solvated electrons (e_{solv}^-) should react faster with the molecules containing electron-poor regions. Taking this fact into account, the decay rate of e_{solv}^- with the 4-OCF_3SQ derivative (lower electron density in the π-system) should be higher than the decay rates with the 4-CH_3SQ, 4-OCH_3SQ and 4-N$(CH_3)_2$-SQ derivatives (higher electron density in the π-system) if the reaction center was only limited to the styryl moiety (aromatic ring, in particular). However, the observed rate constants in Table 3 show the opposite trend. Moreover, a close inspection of the rate constants shows that they are quite similar. Because the differences seem to be not significant, one could assume that the solvated electron attacks primarily the quinoxaline-2-one moiety. Because the substitution occurs at the peripheral positions of the quinoxaline-2-one ring, this cannot affect much the rate constants.

The molar absorption coefficients at the respective maxima of radical anions were calculated to be in the range of 8500−13 100 M^{-1} cm^{-1} (for the first maximum) and of 6100−10 300 (for the second absorption maximum) (Table 6) taking the *G*-value of the reducing species of 0.1067 μM J^{-1} in acetonitrile.[40] These relatively high values of molar absorption coefficients are in line with the calculated oscillator strengths (f) at the respective maxima of radical anions presented in Table 4.

Table 6. Molar Absorption Coefficients of Radical Anions 3-SQ$^{\bullet-}$ Derived from 3-Styryl-quinoxalin-2(1*H*)-one Derivatives (3-SQ)

radical anion 3-SQ$^{\bullet-}$	ε_{max} [a] (M^{-1} cm^{-1})	ε_{max} [b] (M^{-1} cm^{-1})
SQ$^{\bullet-}$	13 100	7500
4-CH_3SQ$^{\bullet-}$	12 200	7000
4-OCH_3SQ$^{\bullet-}$	10 300	6100
4-N$(CH_3)_2$SQ$^{\bullet-}$	8500	7500
4-OCF_3SQ$^{\bullet-}$	13 100	9400
3,4-$(OCH_3)_2$SQ$^{\bullet-}$	12 200	7500
2,5-$(OCH_3)_2$SQ$^{\bullet-}$	10 300	10 300

[a]Calculated for the absorption maxima located at λ = 470−490 nm. [b]Calculated for the absorption maxima located at λ = 510−540 nm.

The same procedure for calculations of molar absorption coefficients (ε) cannot be applied for 3-SQ$^{\bullet-}$ in 2-propanol solutions because of its overlap with the absorption spectrum of e_{solv}^- and also because of its fast protonation (see Protonated Radical Anions) in this solvent. All radical anions 3-SQ$^{\bullet-}$ in acetonitrile decay in a strictly first-order process with k-values lying in the range of 1.2 to 1.5 × 10^6 s^{-1} (Table 2).

Protonated Radical Anions (Hydrogenated Radicals) (3-SQH$^{\bullet}$). The observed absorption spectra in Ar-saturated 2-propanol solutions and assigned tentatively to the protonated

DOI: 10.1021/acs.jpcb.8b01004
J. Phys. Chem. B 2018, 122, 4051−4066

radical anions of 3-styryl-quinoxalin-2(1*H*)-one derivatives (3-SQH$^{\bullet}$) are characterized by a weak single absorption maximum located in the range of 480−490 nm with an accompanying shoulder on the UV side located in the range of 435−470 nm (Table 1).

The protonated radical anions can be formed from the respective radical anions by protonation at N4-atom involving either 2-propanol molecules and/or solvated protons formed during radiolysis of 2-propanol (reaction 2):

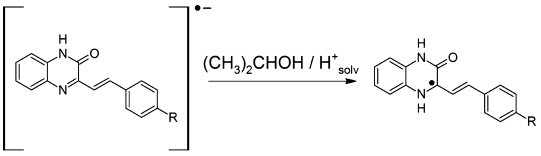

(2)

These radicals decay further in a pseudo-first-order process with k values ranging from 3.7×10^3 s^{-1} (for 4-CH_3SQH$^{\bullet}$) to 8.6×10^3 s^{-1} (for 4-N$(CH_3)_2$SQH$^{\bullet}$) (Table 3).

Radical Cations. The observed absorption spectra in O_2-saturated acetonitrile solutions and assigned to radical cations of 3-styryl-quinoxalin-2(1*H*)-one derivatives (3-SQ$^{\bullet+}$) are characterized by a single broad and intensive absorption maxima located in the range of 450−630 nm. No influence on the position of λ_{max} was observed for $-OCF_3$ and $-CH_3$ substituents, whereas for single and double $-OCH_3$ substituents, a bathochromic shift of $\lambda_{max} \approx 40-60$ nm was observed as compared to the position of λ_{max} for the nonsubstituted 3-styryl-quinoxalin-2-one derivative. In turn, a substantial influence on the position of λ_{max} was found for the N$(CH_3)_2$ substituent with a bathochromic shift of 180 nm (Table 1).

3-Styryl-quinoxalin-2(1*H*)-one derivatives can be considered either as styrene derivatives in which one of H-atoms is substituted by quinoxalin-2(1*H*)-one (R_1 in structure A) or as a quinoxalin-2(1*H*)-one in which a H-atom attached to the C3-atom is substituted by one of the styrene derivatives (R_2 in structure B) (Chart 2).

Chart 2. Structures of 3-Styryl-quinoxalin-2(1*H*)-one Derivatives

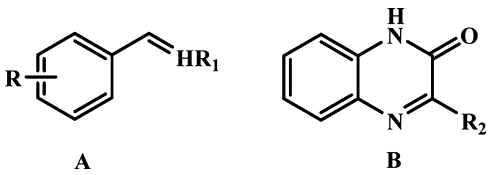

Interestingly, styrene derivatives with R = H and R_1 = H (a), R = CH_3 and R_1 = H (b), R = H and R_1 = CH_3 (c), R = OCH_3 and R_1 = H (d), and R = OCH_3 and R_1 = CH_3 (e) are characterized by two absorption maxima, first intensive located in the range of 350−385 nm and second, much weaker, located in the range 590−620 nm.[62] Comparison of these spectral characteristics with those observed for 3-SQ$^{\bullet+}$ clearly point out that delocalization of a positive charge in 3-SQ$^{\bullet+}$ is not limited to the styrene moiety. Furthermore, the spectral characteristics of radical cations derived from toluene (λ_{max} = 285 and 430 nm),[64] methoxybenzene (λ_{max} = 280 and 430 nm),[65] and *N*-dimethylaniline (λ_{max} = 270 and 465 nm)[66] show clearly that delocalization of a positive charge is also not limited to the substituted benzene moiety (in structure A). Replacement of the substituted styryl moieties by the methyl group at C3-carbon atom of quinoxaline-2(1*H*)-one affects significantly the position of λ_{max}, which shows a hypsochromic shift to λ_{max} = 375 nm (vide supra). This observation points out that delocalization of the positive charge is also not limited to the quinoxaline-2(1*H*)-one moiety. All of these facts mentioned above strongly suggest that delocalization of the positive charge in 3-SQ$^{\bullet+}$ is not limited to the specific moiety but involves the whole molecule.

Calculated spectral parameters of radical cations derived from 3-styryl-quinoxalin-2(1*H*)-one derivatives (3-SQ$^{\bullet+}$) show a very good agreement with the experimentally measured electronic transitions in the maxima for SQ$^{\bullet+}$, 4-CH_3SQ$^{\bullet+}$, and 4-OCF_3SQ$^{\bullet+}$ radical cations. These three molecules show a strong vertical excitation with $\pi \rightarrow \pi^*$ character, and the main contribution comes from a HOMO$_\alpha$ → LUMO$_\alpha$ transition (Figures S15 and S16 in the Supporting Information). Furthermore, CH_3 and OCF_3 substitutions at the para position in the styryl moiety do not alter significantly the frontier MOs with respect to SQ$^{\bullet+}$ (Figure S15 in the Supporting Information). This fact could explain why the maximum of the main absorption band for 4-CH_3SQ$^{\bullet+}$ and 4-OCF_3SQ$^{\bullet+}$ do not shift from λ = 450 nm, the λ_{max} observed for SQ$^{\bullet+}$ (Table 1). The TDDFT gives a fairly good agreement for the 4-OCH_3SQ$^{\bullet+}$ radical cation (Table 1), and the transition with the largest oscillator strength has also $\pi \rightarrow \pi^*$ character (Figure S15). On the other hand, a poor agreement for 4-N$(CH_3)_2$SQ$^{\bullet+}$, 3,4-$(OCH_3)_2$SQ$^{\bullet+}$, and 2,5-$(OCH_3)_2$SQ$^{\bullet+}$ was obtained at this level of theory. This could be caused by a well-known limitation of TDDFT when it is used with generalized gradient approximation or hybrid exchange−correlation functionals.[67] Transitions involving occupied and virtual orbitals with poor spatial overlap tend to give large errors for vertical excitation energies. Close inspection of the MOs for 4-N$(CH_3)_2$SQ$^{\bullet+}$, 3,4-$(OCH_3)_2$SQ$^{\bullet+}$, and 2,5-$(OCH_3)_2$SQ$^{\bullet+}$ reveals that LUMO$_\beta$ is located on the styryl moiety, whereas LUMO$_\alpha$ is delocalized over the whole molecular framework. This fact indicates that using a long-range corrected functional such as CAM-B3LYP will likely give a better correlation with the experimental spectra. Therefore, these three radical cations were studied in vacuum using CAM-B3LYP/def2-TVZP. As expected, improved correlation with the experimental spectra was found for two dimethoxy derivatives 3,4-$(OCH_3)_2$SQ$^{\bullet+}$ and 2,5-$(OCH_3)_2$SQ$^{\bullet+}$, showing the strongest excitation located at λ = 502 and 494 nm, respectively (Table S4), which are much closer to the experimental observations (Table 1). On the other hand, for 4-N$(CH_3)_2$SQ$^{\bullet+}$, a poor correlation with experiment was maintained. For that reason, a higher level of theory is required to treat this molecule; however, this is a complicated task because of its large number of electrons.

In conclusion, as opposed to radical anions, the electron density of radical cations is more influenced by substitution because their ground states are stabilized by electron-donating groups such as $-CH_3$, $-OCH_3$, and $-N(CH_3)_2$, resulting in the larger bathochromic shifts of 25, 40, and 180 nm, respectively. The states involved in the electronic transitions are stabilized because of delocalization of the charge over the whole molecule. In effect, the electronic transitions for the radical cations involve HOMO orbitals located in the quinoxaline-2-one moiety and LUMO orbitals located in the styryl moiety.

Moreover, Hammett σ parameters reflecting inductive and resonance effects of substituents were determined for neutral

DOI: 10.1021/acs.jpcb.8b01004
J. Phys. Chem. B 2018, 122, 4051−4066

molecules in the ground state. Therefore, one can expect that substituents might affect differently ion-radical species where even the charges are different.

The radical cations can be formed by charge transfer from the acetonitrile radical cation to 3-SQ in Ar- and O_2-saturated acetonitrile solutions (reaction 3)

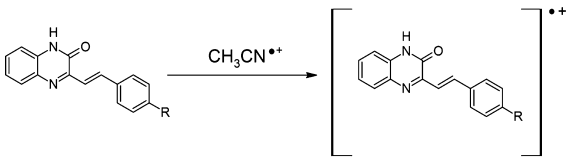

(3)

On the basis of the respective pseudo-first-order rate constants measured for the formation of 3-$SQ^{\bullet+}$ in O_2-saturated acetonitrile solutions containing 0.1 mM 3-SQ (Table 2), the rate constants for reaction 2 were estimated to be in the range $(2.7-4.7) \times 10^9$ M^{-1} s^{-1}. These values are nearly the same as the values measured for analogous reactions involving two 2,3-dihydrooxoisoaporphine derivatives.[43] This might suggest that ionization potentials are also nearly the same for these two classes of heterocyclic compounds. It should also be noted that the formation of 3-$SQ^{\bullet+}$ occurs with slower kinetics in comparison to the formation kinetics of the respective 3-$SQ^{\bullet-}$ (see panels A in Figures 1 and S1–S6) and remains essentially unchanged upon O_2 saturation (see Table 2). This observation is again in agreement with previous pulse radiolysis studies of radical ions derived from oxoisoaporphines[43] and retinal[38] in acetonitrile.

Because a substitution at the para position had an influence on the rate constants of reaction 3 (see Table 2), though weak, an attempt was made to plot the logarithm of the ratio of the rate constants for reaction 3 for substituted 3-SQs and the unsubstituted SQ versus σ constants for each substituent (Figure 5).

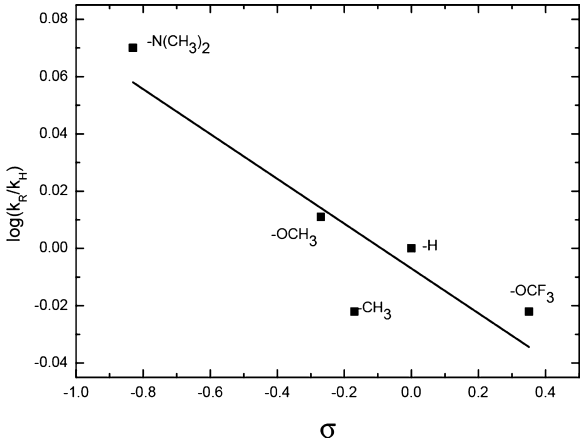

Figure 5. Hammett equation plot of log (k_R/k_H) for charge-transfer reaction between substituted 3-styryl-quinoxalin-2(1*H*)-one derivatives (3-SQ) and a radical cation derived from acetonitrile ($ACN^{\bullet+}$) vs σ parameter. The least-squares treatment gives $\rho = -0.08 \pm 0.02$.

A relatively good correlation is obtained; however, the very small negative slope of this correlation $\rho = -0.08$ indicates and simultaneously confirms a very weak influence of the substituents in the benzene ring on the charge-transfer reaction between a radical cation derived from acetonitrile ($ACN^{\bullet+}$) and substituted 3-styryl-quinoxalin-2(1*H*)-one derivatives (4R-3SQ).

It should be noted that, in principle, the pseudo-first-order rate constants calculated for the first exponential decay (which can be assigned to the decay of 3-$SQ^{\bullet+}$) are not affected by saturation with O_2, which suggests a complete charge–spin delocalization in the radical cations. A slight increase (≈20–25%) was only observed for 4-$OCH_3SQ^{\bullet+}$, 4-$OCF_3SQ^{\bullet+}$, and 3,4-$OCH_3SQ^{\bullet+}$ (see Table 2). This observation is in line with the earlier observation for radical cations of *trans*-stilbene containing a methoxy group in the para position, which revealed a relatively small reactivity toward O_2 with k(*t*-$St^{\bullet+}$ + O_2) = $(1.2-4.5) \times 10^7$ M^{-1} s^{-1}. It was concluded that *p*-methoxy substitution causes separation and localization of the positive charge on the oxygen atom of the $-OCH_3$ group and an unpaired electron on the olefinic β-carbon (charge–spin separation), forming a quinoid-type structure.[35,36,68] However, such charge–spin separation seems to be not important for 3-$SQ^{\bullet+}$, even for 4-$OCH_3SQ^{\bullet+}$ and 4-$OCF_3SQ^{\bullet+}$, which revealed a very small reactivity toward O_2 with $k < 5 \times 10^6$ M^{-1} s^{-1}. This suggests that the barrier to the twisting of the C=C double bond in 3-$SQ^{\bullet+}$ is very high.

CONCLUSIONS

In the current paper, application of pulse radiolysis as a method of generation of radical ions allowed selective generation and observation of radical anions and cations derived from 3-styryl-quinoxalin-2(1*H*)-one derivatives.

The experimental spectra of the "isolated" radical anions were reproduced adequately by semiempirical quantum mechanical calculations performed previously using ZINDO/S on the optimized PM3 geometry. A good reproduction of experimental spectra of radical cations 4R-$SQ^{\bullet+}$ (for R = H, CH_3, OCH_3, and OCF_3) was obtained using TDDFT methods, whereas for 3,4-$(OCH_3)_2SQ^{\bullet+}$ and 2,5-$(OCH_3)_2SQ^{\bullet+}$, a long-range corrected functional CAM-B3LYP was additionally applied.

Our current findings, especially those addressing the spectral properties of radical anions and hydrogenated radicals, will be useful for interpretation of spectral data obtained during photoreduction of 3-styryl-quinoxalin-2-one derivatives, which are currently in progress.

ASSOCIATED CONTENT

Supporting Information

The Supporting Information is available free of charge on the ACS Publications website at DOI: 10.1021/acs.jpcb.8b01004.

Absorption spectra recorded in Ar- and O_2-saturated acetonitrile solutions containing 0.1 mM **1b–1g** compounds; absorption spectra recorded in Ar-saturated 2-propanol solutions containing 0.1 mM **1b–1g** compounds; absorption spectra recorded in Ar-saturated acetonitrile solutions containing 0.1 mM 3-methylquinoxalin-2(1*H*)-one; absorption spectra recorded in O_2-saturated acetonitrile solutions containing 0.1 mM 3-methylquinoxalin-2(1*H*)-one; MOs involved in the electronic transitions for 3-$SQ^{\bullet+}$; formation enthalpies for the 3-$SQH^{\bullet}$ radicals; M06-2x/def2-TZVP-calculated vertical excitation energies for 3-$SQ^{\bullet+}$; CAM-B3LYP/def2-TZVP-calculated vertical excitation energies for 2,5$(OCH_3)_2$-$SQ^{\bullet+}$; 3,4$(OCH_3)_2$-$SQ^{\bullet+}$; and 4-NCH_3-

DOI: 10.1021/acs.jpcb.8b01004
J. Phys. Chem. B 2018, 122, 4051–4066

$SQ^{\bullet+}$; and spectral characterization of **1a**−**1g** by ^1H NMR and HRMS-ESI (+mode) (PDF)

AUTHOR INFORMATION

Corresponding Authors

*E-mail: jrfuente@ciq.uchile.cl. Phone: (56-2) 2978-2880. Fax: (56-2)-2978-2868 (J.R.D.l.F.).

*E-mail: k.bobrowski@ichtj.waw.pl. Phone: (48-22)-504-1336 (K.B.).

ORCID

Krzysztof Bobrowski: 0000-0002-7791-9184

Notes

The authors declare no competing financial interest.

ACKNOWLEDGMENTS

Financial support under FONDECYT grant no. 1150567 which made possible exchange scientific visits of J.R.D.l.F. and K.B. in the INCT (Warsaw, Poland) and the Universidad de Chile (Santiago, Chile), respectively, is greatly acknowledged. Two of us would like to acknowledge the Polish National Center of Science (NCN) for PRELUDIUM grant no. 2014/15/N/ST4/02914 (K.S.) and the US Department of Energy Office of Science, Office of Basic Energy Science, under award number DE-FC02-04ER15533 (K.B.). This is document number NDRL-5201 from the Notre Dame Radiation Laboratory.

REFERENCES

(1) Pereira, J. A.; Pessoa, A. M.; Cordeiro, M. N. D. S.; Fernandes, R.; Prudêncio, C.; Noronha, J. P.; Vieira, M. Quinoxaline, its Derivatives and Applications: A State of the Art Review. *Eur. J. Med. Chem.* **2015**, *97*, 664−672.

(2) Obot, I. B.; Obi-Egbedi, N. O.; Odozi, N. W. Acenaphtho[1,2-b]quinoxaline as a Novel Corrosion Inhibitor for Mild Steel in 0.5 M H_2SO_4. *Corros. Sci.* **2010**, *52*, 923−926.

(3) Achelle, S.; Baudequin, C.; Plé, N. Luminescent Materials Incorporating Pyrazine or Quinoxaline Moieties. *Dyes Pigm.* **2013**, *98*, 575−600.

(4) Wang, P.; Xie, Z.; Hong, Z.; Tang, J.; Wong, O.; Lee, C.-S.; Wong, N.; Lee, S. Synthesis, Photoluminescence and Electroluminescence of New 1*H*-Pyrazolo[3,4-b]quinoxaline Derivatives. *J. Mater. Chem.* **2003**, *13*, 1894−1899.

(5) Wang, P.; Xie, Z.; Wong, O.; Lee, C.-.-S.; Wong, N.; Hung, L.; Lee, S. New 1H-Pyrazolo[3,4-b]quinoxaline Derivatives as Sharp Green-Emitting Dopants for Highly Efficient Electroluminescent Devices. *Chem. Commun.* **2002**, 1404−1405.

(6) Thomas, K. R. J.; Velusamy, M.; Lin, J. T.; Chuen, C.-H.; Tao, Y.-T. Chromophore-Labeled Quinoxaline Derivatives as Efficient Electroluminescent Materials. *Chem. Mater.* **2005**, *17*, 1860−1866.

(7) Chen, C.-T.; Lin, J.-S.; Moturu, M. V. R. K.; Lin, Y.-W.; Yi, W.; Tao, Y.-T.; Chien, C.-H. Doubly *Ortho*-linked Quinoxaline/Triarylamine Hybrid as a Bifunctional, Dipolar Electroluminescent Template for Optoelectronic Applications. *Chem. Commun.* **2005**, 3980−3982.

(8) Siram, R. B. K.; Smith, J.; Anthopoulos, T. D.; Patil, S. Acenaphtho[1,2-b]quinoxaline Based Low Band Gap Copolymers for Organic Thin Film Transistor Applications. *J. Mater. Chem.* **2012**, *22*, 4450−4458.

(9) Ajani, O. O. Present Status of Quinoxaline Motifs: Excellent Pathfinders in Therapeutic Medicine. *Eur. J. Med. Chem.* **2014**, *85*, 688−715.

(10) Carta, A.; Piras, S.; Loriga, G.; Paglietti, G. Chemistry, Biological Properties and SAR Analysis of Quinoxalinones. *Mini-Rev. Med. Chem.* **2006**, *6*, 1179−1200.

(11) Mikiciuk-Olasik, E.; Trzebinski, P.; Nowak, R.; Kotelko, B. Synthesis of New Derivatives of 4-Acylquinoxalin-2-ones with Potential Pharmacological Activity. *Acta Pol. Pharm.* **1994**, *51*, 231−233.

(12) Carta, A.; Sanna, P.; Loriga, M.; Setzu, M. G.; La Colla, P.; Loddo, R. Synthesis and Evaluation for Biological Activity of 3-Alkyl and 3-Halogenoalkyl-quinoxalin-2-ones Variously Substituted. Part 4. *Il Farmaco* **2002**, *57*, 19−25.

(13) Hussain, S.; Parveen, S.; Hao, X.; Zhang, S. D.; Wang, W.; Qin, X.; Yang, Y. S.; Chen, X.; Zhu, S.; Ahu, C.; Ma, B. Structure-Activity Relationships Studies of Quinoxalinone Derivatives as Aldose Reductase Inhibitors. *Eur. J. Med. Chem.* **2014**, *80*, 383−392.

(14) Qin, X.; Hao, X.; Han, H.; Zhu, S.; Yang, Y.; Wu, B.; Hussain, S.; Parveen, S.; Jing, C.; Ma, B.; Zhu, C. Design and Synthesis of Potent and Multifunctional Aldose Reductase Inhibitors Based on Quinoxalinones. *J. Med. Chem.* **2015**, *58*, 1254−1267.

(15) Kawanishi, N.; Sugimoto, T.; Shibata, J.; Nakamura, K.; Masutani, K.; Ikuta, M.; Hirai, H. Structure-Based Drug Design of a Highly Potent CDK1,2,4,6 Inhibitor with Novel Macrocyclic Quinoxalin-2-one Structure. *Bioorg. Med. Chem. Lett.* **2006**, *16*, 5122−5126.

(16) Khattab, S. N.; Hassan, S. Y.; Bekhit, A. A.; El Massry, A. M.; Langer, V.; Amer, A. Synthesis of New Series of Quinoxaline Based MAO-Inhibitors and Docking Studies. *Eur. J. Med. Chem.* **2010**, *45*, 4479−4489.

(17) Székelyhidi, Z.; Pató, J.; Wáczek, F.; Bánhegyi, P.; Hegymegi-Barakonyi, B.; Eros, D.; Mészáros, G.; Hollósy, F.; Hafenbradl, D.; Obert, S.; Klebl, B.; Kéri, G.; Orfi, L. Synthesis of Selective SRPK-1 Inhibitors: Novel Tricyclic Quinoxaline Derivatives. *Bioorg. Med. Chem. Lett.* **2005**, *15*, 3241−3246.

(18) Dudash, J.; Zhang, Y.; Moore, J. B.; Look, R.; Liang, Y.; Beavers, M. P.; Conway, B. R.; Rybczynski, P. J.; Demarest, K. T. Synthesis and Evaluation of 3-Anilino-Quinoxalinones as Glycogen Phosphorylase Inhibitors. *Bioorg. Med. Chem. Lett.* **2005**, *15*, 4790−4793.

(19) Kim, K. S.; Qian, L.; Bird, J. E.; Dickinson, K. E. J.; Moreland, S.; Schaeffer, T. R.; Waldron, T. L.; Delaney, C. L.; Weller, H. N.; Miller, A. V. Quinoxaline N-Oxide Containing Potent Angiotensin II Receptor Antagonists: Synthesis, Biological Properties, and Structure-Activity Relationships. *J. Med. Chem.* **1993**, *36*, 2335−2342.

(20) Lawrence, D. S.; Copper, J. E.; Smith, C. D. Structure-Activity Studies of Substituted Quinoxalinones as Multiple-Drug-Resistance Antagonists. *J. Med. Chem.* **2001**, *44*, 594−601.

(21) Campiani, G.; Morelli, E.; Gemma, S.; Nacci, V.; Butini, S.; Hamon, M.; Novellino, E.; Greco, G.; Cagnotto, A.; Goegan, M.; Cervo, L.; Dalla Valle, F.; Fracasso, C.; Caccia, S.; Mennini, T. Pyrroloquinoxaline Derivatives as High-Affinity and Selective 5-HT3 Receptor Agonists: Synthesis, Further Structure-Activity Relationships, and Biological Studies. *J. Med. Chem.* **1999**, *42*, 4362−4379.

(22) TenBrink, R. E.; Im, W. B.; Sethy, V. H.; Tang, A. H.; Carter, D. B. Antagonist, Partial Agonist, and Full Agonist Imidazo[1,5-a]quinoxaline Amides and Carbamates Acting through the GABAA/Benzodiazepine Receptor. *J. Med. Chem.* **1994**, *37*, 758−768.

(23) Jacobsen, E. J.; TenBrink, R. E.; Stelzer, L. S.; Belonga, K. L.; Carter, D. B.; Im, H. K.; Im, W. B.; Sethy, V. H.; Tang, A. H.; VonVoigtlander, P. F.; Petke, J. D. High-Affinity Partial Agonist Imidazo[1,5-a]quinoxaline Amides, Carbamates, and Ureas at the γ-Aminobutyric Acid A/Benzodiazepine Receptor Complex. *J. Med. Chem.* **1996**, *39*, 158−175.

(24) Mickelson, J. W.; Jacobsen, E. J.; Carter, D. B.; Im, H. K.; Im, W. B.; Schreur, P. J. K. D.; Sethy, V. H.; Tang, A. H.; McGee, J. E.; Petke, J. D. High-Affinity α-Aminobutyric Acid A/Benzodiazepine Ligands: Synthesis and Structure-Activity Relationship Studies of a New Series of Tetracyclic Imidazoquinoxalines. *J. Med. Chem.* **1996**, *39*, 4654−4666.

(25) Jacobsen, E. J.; Stelzer, L. S.; TenBrink, R. E.; Belonga, K. L.; Carter, D. B.; Im, H. K.; Im, W. B.; Sethy, V. H.; Tang, A. H.; VonVoigtlander, P. F.; Petke, J. D.; Zhong, W.-Z.; Mickelson, J. W. Piperazine Imidazo[1,5-a]quinoxaline Ureas as High-Affinity GABAA Ligands of Dual Functionality. *J. Med. Chem.* **1999**, *42*, 1123−1144.

(26) Wagle, S.; Adhikari, A. V.; Kumari, N. S. Synthesis of Some New 4-Styryltetrazolo[1,5-a]quinoxaline and 1-Substituted-4-Styryl[1,2,4]-

DOI: 10.1021/acs.jpcb.8b01004
J. Phys. Chem. B 2018, 122, 4051−4066

triazolo[4,3-a]quinoxaline Derivatives as Potent Anticonvulsants. *Eur. J. Med. Chem.* **2009**, *44*, 1135−1143.
(27) Noolvi, M. N.; Patel, H. M.; Bhardwaj, V.; Chauhan, A. Synthesis and in vitro Antitumor Activity of Substituted Quinazoline and Quinoxaline Derivatives: Search for Anticancer Agent. *Eur. J. Med. Chem.* **2011**, *46*, 2327−2346.
(28) Liu, L.; Zhang, L.; Wang, T.; Liu, M. Interfacial Assembly of Amphiphilic Styrylquinoxalines: Alkyl Chain Length Tunable Topochemical Reactions and Supramolecular Chirality. *Phys. Chem. Chem. Phys.* **2013**, *15*, 6243−6249.
(29) Ma, Y.; Lin, L.; Zhang, L.; Liu, M.; Guo, Y.; Lu, Z. Effect of Acidity on Morphologies and Photodimerization Kinetics in Langmuir-Blodgett Monolayers of Styrylquinoline Derivatives. *Chin. Chem. Lett.* **2017**, *28*, 1285−1289.
(30) Yin, M.; Gong, H.; Zhang, B.; Liu, M. Photochemical Reaction, Acidichromism, and Supramolecular Nanoarchitectures in the Langmuir−Blodgett Films of an Amphiphilic Styrylquinoxaline Derivative. *Langmuir* **2004**, *20*, 8042−8048.
(31) Benzeid, H.; Mothes, E.; Essassi, E. M.; Faller, P.; Pratviel, G. A Thienoquinoxaline and a Styryl-Quinoxaline as New Fluorescent Probes for Amyloid-β Fibrils. *C. R. Chim.* **2012**, *15*, 79−85.
(32) Kinoshita, T.; Miyake, H.; Fujii, T.; Takakura, S.; Goto, T. The Structure of Human Recombinant Aldose Reductase Complexed with the Potent Inhibitor Zenarestat. *Acta Crystallogr., Sect. D: Biol. Crystallogr.* **2002**, *58*, 622−626.
(33) Skotnicki, K.; De la Fuente, J. R.; Cañete, A.; Bobrowski, K. Radiation-Induced Reduction of Quinoxalin-2-one Derivatives in Aqueous Solutions. *Radiat. Phys. Chem.* **2016**, *124*, 91−98.
(34) Skotnicki, K.; De la Fuente, J. R.; Cañete, A.; Bobrowski, K. Spectral and Kinetic Properties of Radicals Derived from Oxidation of Quinoxalin-2-one and its Methyl Derivative. *Molecules* **2014**, *19*, 19152−19171.
(35) Majima, T.; Tojo, S.; Ishida, A.; Takamuku, S. Reactivities of Isomerization, Oxidation, and Dimerization of Radical Cations of Stilbene Derivatives. *J. Phys. Chem.* **1996**, *100*, 13615−13623.
(36) Majima, T.; Tojo, S.; Ishida, A.; Takamuku, S. *Cis-Trans* Isomerization and Oxidation of Radical Cations of Stilbene Derivatives. *J. Org. Chem.* **1996**, *61*, 7793−7800.
(37) Bobrowski, K.; Dzierzkowska, G.; Grodkowski, J.; Stuglik, Z.; Zagórski, Z. P.; McLaughlin, W. L. A Pulse Radiolysis Study of the Leucocyanide of Malachite Green Dye in Organic Solvents. *J. Phys. Chem.* **1985**, *89*, 4358−4366.
(38) Bobrowski, K.; Das, P. K. Transient Phenomena in the Pulse Radiolysis of Retinyl Polyenes. 4. Environmental Effects on Absorption Maximum of Retinal Radical Anion. *J. Phys. Chem.* **1985**, *89*, 5733−5738.
(39) Baptista, J. L.; Burrows, H. D. Solute Ion and Radical Formation in the Pulse Radiolysis of Acetonitrile Solutions. *J. Chem. Soc., Faraday Trans. 1* **1974**, *70*, 2066−2079.
(40) Bell, I. P.; Rodgers, M. A. J.; Burrows, H. D. Kinetic and Thermodynamic Character of Reducing Species Produced on Pulse Radiolysis of Acetonitrile. *J. Chem. Soc., Faraday Trans. 1* **1977**, *73*, 315−326.
(41) Burrows, H. D.; Kosower, E. M. Optical spectra and Reactivities of Radical Anions of 4-Nitrobenzyl Compounds Produced by Pulse Radiolysis of Acetonitrile Solutions. *J. Phys. Chem.* **1974**, *78*, 112−117.
(42) Tran-Thi, T. H.; Koulkes-Pujo, A. M.; Gilles, L.; Genies, M.; Sutton, J. Transient Species Formed by Pulse Radiolysis of Solutions of N-Methylacetamide (NMA) in Methyl Cyanide. *Radiat. Phys. Chem.* **1980**, *15*, 209−214.
(43) De la Fuente, J. R.; Kciuk, G.; Sobarzo-Sanchez, E.; Bobrowski, K. Transient Phenomena in the Pulse Radiolysis of Oxoisoaporphine Derivatives in Acetonitrile. *J. Phys. Chem. A* **2008**, *112*, 10168−10177.
(44) Doan, S. C.; Schwartz, B. J. Ultrafast Studies of Excess Electrons in Liquid Acetonitrile: Revisiting the Solvated Electron/Solvent Dimer Anion Equilibrium. *J. Phys. Chem. B* **2013**, *117*, 4216−4221.
(45) Doan, S. C.; Schwartz, B. J. Nature of Excess Electrons in Polar Fluids: Anion-Solvated Electron Equilibrium and Polarized Hole-Burning in Liquid Acetonitrile. *J. Phys. Chem. Lett.* **2013**, *4*, 1471−1476.
(46) Shkrob, I. A.; Sauer, M. C. Electron Localization in Liquid Acetonitrile. *J. Phys. Chem. A* **2002**, *106*, 9120−9131.
(47) Timerghazin, Q. K.; Peslherbe, G. H. Electronic Structure of the Acetonitrile and Acetonitrile Dimer Anions: A Topological Investigation. *J. Phys. Chem. B* **2008**, *112*, 520−528.
(48) Raghavan, N. V.; Das, P. K.; Bobrowski, K. Transient Phenomena in the Pulse Radiolysis of Retinyl Polyenes. 1. Radical Anions. *J. Am. Chem. Soc.* **1981**, *103*, 4569−4573.
(49) Bobrowski, K.; Das, P. K. Transient Phenomena in the Pulse Radiolysis of Retinyl Polyenes. 3. Radical Cations. *J. Phys. Chem.* **1985**, *89*, 5079−5085.
(50) Dorfman, L. M. Electron and Proton Transfer Reactions of Aromatic Molecule Ions in Solution. *Acc. Chem. Res.* **1970**, *3*, 224−230.
(51) De la Fuente, J. R.; Neira, V.; Saitz, C.; Jullian, C.; Sobarzo-Sanchez, E. Photoreduction of Oxoisoaporphine Dyes by Amines: Transient-Absorption and Semiempirical Quantum-Chemical Studies. *J. Phys. Chem. A* **2005**, *109*, 5897−5904.
(52) De la Fuente, J. R.; Cañete, Á.; Jullian, C.; Saitz, C.; Aliaga, C. Unexpected Imidazoquinoxalinone Annulation Products in the Photoinitiated Reaction of Substituted-3-Methyl-Quinoxalin-2-ones with N-Phenylglycine. *Photochem. Photobiol.* **2013**, *89*, 1335−1345.
(53) Mirkowski, J.; Wisniowski, P.; Bobrowski, K. *INCT Annual Report 2000*; INCT, 2001.
(54) Bobrowski, K. Free Radicals in Chemistry, Biology and Medicine: Contribution of Radiation Chemistry. *Nukleonika* **2005**, *50*, S67−S76.
(55) Hug, G. L.; Wang, Y.; Schöneich, C.; Jiang, P.-Y.; Fessenden, R. W. Multiple Time Scales in Pulse Radiolysis. Application to Bromide Solutions and Dipeptides. *Radiat. Phys. Chem.* **1999**, *54*, 559−566.
(56) Zhao, Y.; Truhlar, D. G. The M06 Suite of Density Functionals for Main group Thermochemistry, Thermochemical Kinetics, Noncovalent Interactions, Excited States, and Transition Elements: Two New Functionals and Systematic Testing of Four M06-Class functionals and 12 other functionals. *Theor. Chem. Acc.* **2008**, *120*, 215−241.
(57) Weigend, F.; Ahlrichs, R. Balanced Basis Sets of Split Valence, Triple Zeta Valence and Quadruple Zeta Valence Quality for H to Rn: Design and Assessment of Accuracy. *Phys. Chem. Chem. Phys.* **2005**, *7*, 3297−3305.
(58) Klamt, A.; Schüürmann, G. COSMO: A New Approach to Dielectric Screening in Solvents with Explicit Expressions for the Screening Energy and its Gradient. *J. Chem. Soc., Perkin Trans. 2* **1993**, 799−805.
(59) *TURBOMOLE*, V7.0 2015. http://www.turbmole.com, 1989−2007.
(60) Yanai, T.; Tew, D. P.; Handy, N. C. A New Hybrid Exchange−Correlation Functional Using the Coulomb-Attenuating Method (CAM-B3LYP). *Chem. Phys. Lett.* **2004**, *393*, 51−57.
(61) Valiev, M.; Bylaska, E. J.; Govind, N.; Kowalski, K.; Straatsma, T. P.; van Dam, H. J. J.; Wang, D.; Nieplocha, J.; Apra, E.; Windus, T. L.; de Jong, W. A. NWChem: A Comprehensive and Scalable Open-Source Solution for Large Scale Molecular Simulations. *Comput. Phys. Commun.* **2010**, *181*, 1477−1489.
(62) Brede, O.; David, F.; Steenken, S. Photo- and Radiation-Induced Chemical Generation and Reactions of Styrene Radical Cations in Polar and Non-Polar Solvents. *J. Chem. Soc., Perkin Trans. 2* **1995**, 23−32.
(63) Hansch, C.; Leo, A.; Taft, R. W. A Survey of Hammett Substituent Constants and Resonance and Field Parameters. *Chem. Rev.* **1991**, *91*, 165−195.
(64) Sehested, K.; Holcman, J.; Hart, E. J. Conversion of Hydroxycyclohexadienyl Radicals of Methylated Benzenes to Cation Radicals in Acid Media. *J. Phys. Chem.* **1977**, *81*, 1363−1367.
(65) O'Neill, P.; Steenken, S.; Schulte-Frohlinde, D. Formation of Radical Zwitterions from Methoxylated Benzoic Acids. 2. Hydroxyl Adducts as Precursors. *J. Phys. Chem.* **1977**, *81*, 31−34.

DOI: 10.1021/acs.jpcb.8b01004
J. Phys. Chem. B 2018, 122, 4051−4066

(66) Holcman, J.; Sehested, K. Dissociation of the hydroxyl Adduct of N,N-Dimethylaniline in Aqueous Solution. *J. Phys. Chem.* **1977**, *81*, 1963−1966.
(67) Peach, M. J. G.; Benfield, P.; Helgaker, T.; Tozer, D. J. Excitation Energies in Density Functional Theory: An Evaluation and a Diagnostic Test. *J. Chem. Phys.* **2008**, *128*, 044118.
(68) Tojo, S.; Morishima, K.; Ishida, A.; Majima, T.; Takamuku, S. Remarkable Enhancements of Isomerization and Oxidation of Radical Cations of Stilbene Derivatives Induced by Charge-Spin Separation. *J. Org. Chem.* **1995**, *60*, 4684−4685.

DOI: 10.1021/acs.jpcb.8b01004
J. Phys. Chem. B 2018, 122, 4051−4066